Functionalized peptide hydrogels as tunable extracellular matrix mimics for biological applications

Katharina S. Hellmund, Benjamin Von Lospichl, Christoph Böttcher, Kai Ludwig, Uwe Keiderling, Laurence Noirez, Annika Weiss, Dorian J. Mikolajczak, Michael Gradzielski, Beate Koksch

Functionalized peptide hydrogels as tunable extracellular matrix mimics for biological applications

Katharina S. Hellmund[a]‡, Benjamin von Lospichl[b]‡, Christoph Böttcher[c], Kai Ludwig[c], Uwe Keiderling[d], Laurence Noirez[e], Annika Weiß[a], Dorian J. Mikolajczak[a], Michael Gradzielski[b] and Beate Koksch[a].*

[a] Institute of Chemistry and Biochemistry – Organic Chemistry, Freie Universität Berlin, Takustraße 3, 14195 Berlin (Germany)

[b] Stranski-Laboratory of Physical and Theoretical Chemistry, Institute of Chemistry, Technische Universität Berlin, Straße des 17. Juni 124, 10623 Berlin (Germany)

[c] Institute of Chemistry and Biochemistry and CoreFacility BioSupraMol Freie Universität Berlin, Fabeckstrasse 36a, 14195 Berlin (Germany)

[d] Helmholtz-Zentrum Berlin für Materialien und Energie, Hahn-Meitner-Platz 1, 14109 Berlin (Germany)

[e] Laboratoire Léon Brillouin (CEA-CNRS) Université Paris-Saclay, CE-Saclay, 91190 Gif-sur-Yvette Cédex (France)

KEYWORDS. Extracellular Matrix, Peptide Hydrogel, Coiled coil, SANS

ABSTRACT

The development of tailorable and biocompatible three-dimensional (3D) substrates or molecular networks that reliably mimic the extracellular matrix (ECM) and influence cell behavior and growth *in vitro* is of increasing interest for cell-based applications in the field of tissue engineering and regenerative medicine. In this context, we present a novel coiled coil-based peptide that self-assembles into a 3D-α-helical fibril network and functions as a self-supporting hydrogel. By functionalizing distinct coiled-coil peptides with cellular binding motifs (RGD) or carbohydrate ligands (mannose), and by utilizing the multivalency and modularity of coiled-coil assemblies, tailored artificial ECMs are obtained. Fibrillar network and ligand density, as well as ligand composition can readily be adjusted by changes in water content or peptide concentrations, respectively. Mesoscopic structure of these networks was assessed by rheology and small-angle neutron scattering experiments. Initial cell viability studies using NIH/3T3 cells showed comparable or even superior cell viability using the presented artificial ECMs, compared to commercially available 3D-cell culture scaffold Matrigel®. The herein reported approach presents a reliable (low batch-to-batch variation) and modular pathway towards biocompatible and tailored artificial ECMs.

TEXT.

Extracellular matrices (ECM) are complex three-dimensional (3D) networks of macromolecules that play a pivotal role in processes that direct cell fate and behavior *in vivo*.[1–5] ECMs typically comprise various proteins, including laminin, collagens, elastin, proteoglycans, and an intricate mixture of growth factors, adhesion ligands and other soluble molecules.[6] The sophisticated molecular environment that is generated by the ECM provides

and supports important cellular functions, such as growth, maintenance, and differentiation of various cells. Therefore, the development of synthetic materials that closely resemble the environment of natural ECM, to enable increased cell viability, proliferation and tissue specific differentiation *in vitro* is of increasing interest for medical and clinical applications and tissue engineering.

Various *in vitro* growth materials have been developed based on hydrogels of different polymers or cross-linked carbohydrates.[7] However, the hydrogel formulation of these materials is not applicable to all cell types. Therefore, natural ECM extracts from living cells are widely utilized as they contain advantageous mixtures of structural proteins and growth factors for more sensitive cell-growth conditions.[1] One of the most applied cell culture extracts is commercialized as Matrigel® (BD Biosciences, Mississauga, Canada).[8,9] Albeit, the established success of such extracts from cells as 3D-cell culture matrices, individual extraction batches possess ill-defined compositions and quantities of individual components, which affects experimental performance.[10,11] Moreover, tuning of mechanical or biochemical properties entails the risk for contamination or degradation.[10] Thus, one of our main research goals in this field, which we see as a complementary approach to cell extracts, is the development of a synthetic 3D-cell-culture matrix, which is inherently modular and allows for the presentation of defined amounts of desired (biochemical)ligands, while mechanical properties can readily be fine-tuned.

Chemically synthesized peptide-based materials may present a pathway towards such 3D-matrices. Designed peptides possess the ability to adopt well-defined secondary, tertiary or even higher-ordered quaternary structures and assemble into complex 3D-architectures. The molecular complexity of peptidic structures can be fine-tuned by changes in the primary structure and incorporation of, e.g., non-canonical amino acid building blocks,[12] or by introduction of small molecule ligands or glycans into specific amino acid side chains.[13,14] Peptides can be synthesized with a low batch-to-batch variation in high purity using solid-

phase-peptide-synthesis (SPPS) and their folding behavior into the programmed structures is reliably and reproducible. The potential of peptides to function as 3D-cell culture substrates has already been successfully proven.[15]

Among the plethora of available peptide structures, the α-helical coiled-coil motif is a well-characterized naturally occurring folding motif commonly used in various peptidic model systems.[16] The coiled-coil motif consists of two to seven α-helices that wrap around each other to form a left-handed superhelical twist.[16,17] The primary amino acid sequence is characterized by a repetition of seven amino acids, called heptad repeat.[16] Amino acids within a heptad repeat are denoted as *a-b-c-d-e-f-g*, where positions *a* and *d* are commonly occupied by nonpolar amino acid residues such as leucine, isoleucine, and valine, which form the hydrophobic core of the helix bundle[18,19] that directs the folding and packing of the amphipathic structure.[16] Positions *e* and *g* are occupied mostly by charged amino acids like arginine, glutamic acid and lysine that provide intermolecular ionic interactions between the individual peptide helices and direct orientation of the coiled coil.[17,20] The remaining positions *b*, *c* and *f* are located at the solvent-exposed region at the periphery of the α-helices and are appropriate positions for side chain modifications with, e.g., carbohydrate moieties or peptide ligands.[13,14,17] Individual coiled-coil peptide sequences can be functionalized with diverse ligands, enabling the generation of customized peptide monomers that afterwards assemble into tailored coiled-coil structures. Studies by Hodges *et al.*, Kim *et al*. and Woolfson *et al*., established rules for the design of α-helical peptide bundles with a predictable degree of oligomerization,[21–25] further extending the design scope of these structures. The coiled-coil folding motif has proven to be an advantageous and reliable platform for the generation of many biomaterials that find application in, e.g. tissue engineering[26–29] or as versatile substrates for cell culture experiments.[15]

Woolfsen and coworkers showed that a heterodimeric coiled coil-based hydrogel (hSAFs), which includes more than 99% water (by weight), supports the growth and differentiation of

PC12 cells, however, to a lesser extent than the control substrate Matrigel®.[30] The overall lower growth was associated with the absence of cell-recognition motifs, or growth factors, which are present within Matrigel®.

Another study by Woolfsen and coworkers, reported that the same heterodimeric coiled coil-based self-organizing hSAFs hydrogels, which have been additionally decorated with the RGDS tetrapeptide, a recognition motif from fibronectin,[31] form 3D biomaterials that are able to increase the proliferative activity of embryonic neuronal stem cells (NSCs), thus, support the differentiation of NSCs.[28] This example also highlights the potential of coiled-coil-based 3D-substrates also for stem cell culture.

To tie in with the given background, we designed a peptide sequence, namely hFF03 (Tab. 1) that consist of only four different amino acids and is based on a homomeric coiled-coil dimer. hFF03 self-assembles into stable α-helical fibers and builds up self-supporting hydrogels under physiological conditions as well as enables the presentation of biologically relevant ligands at the same time. Thus, hFF03 was modified with the tripeptide ligand, RGD, as well as with the monosaccharide mannose resulting in three hFF03 variants that can be combined at will to generate tailored artificial ECM. Conjugation of these molecules was achieved by using a previously reported all-on-solid-phase (AOSP) approach, where RGD-sequence and mannose were included by standard solid phase peptide synthesis.[13]

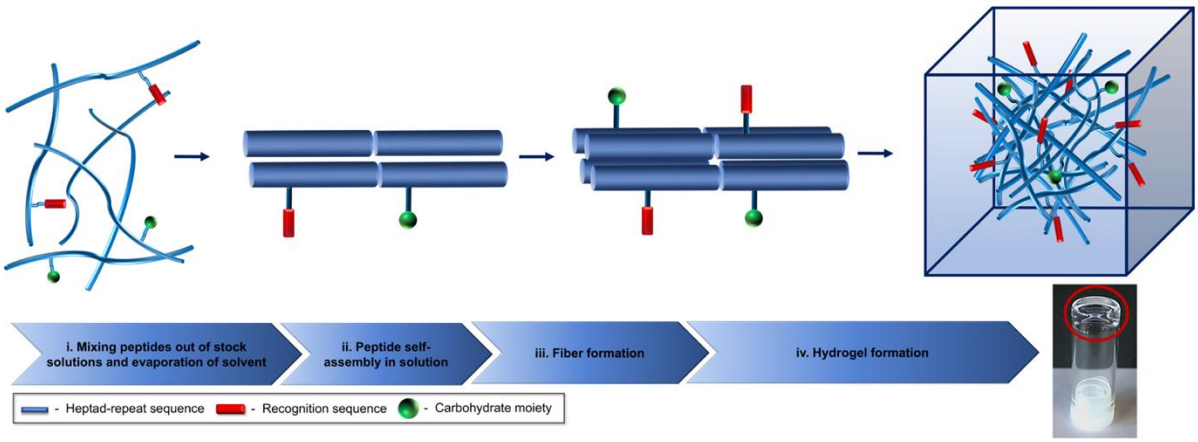

Figure 1. Schematic representation of hydrogel formation by mixing of different ligand presenting coiled coil peptides. Hydrogel formation indicated by inversion of the sample vial (bottom right).[32]

The presented rational design approach utilizes the modularity of the coiled-coil system to enable a systematic study of the structure and stability of hydrogel formation depending on the nature and concentration of a recognition motif (RGD) or carbohydrate ligand (mannose) as well as the combination of both, bound to one 3D scaffold. In the following, hFF03 and its variants are systematically studied, in terms of peptide secondary structure, mechanical properties and cytotoxicity, as pure compounds and as mixtures, in various compositions and concentrations (Table S).

Materials and Methods

Peptide Synthesis

Solid-phase peptide synthesis was performed on resins acquired from Novabiochem. All Fmoc-protected amino acids were purchased from Orpegen. hFF03 and hFF03 variants were synthesized using preloaded Fmoc-Leu-NovaSyn TGA resin (0.2 mmol/g substitution), respectively. Synthesis was performed by standard Fluorenylmethyloxycarbonyl-(Fmoc)-chemistry on a 0.1 mmol scale. Fmoc-deprotection was performed with 2% piperidine and 2%

1,8-Diazabicyclo[5.4.0]undec-7-en (DBU) in DMF (3x7 min using 5 mL of deprotecting solution) at each step.

Synthesis of hFF03 and hFF03-variants was accomplished in two steps: hFF03 was synthesized by performing two coupling steps per amino acid (1 h each coupling) using an automated synthesizer Activo P-11 Automated Peptide Synthesizer (Activotec, Cambridge, United Kingdom) and amino acid (8 eq.), 2-(1H-7-Azabenzotriazol-1-yl)-1,1,3,3-tetramethyluronoium hexafluorphosphate (HATU, 8 eq.), as well as *N*,*N*-diisopropylethylamin (DIPEA, 16 eq.) relative to resin loading. In case of decorated variants of hFF03 tBu-protected lysine in position 17 was substituted for *N*-Methyltrityl-protected (Mtt) lysine purchased from Carbolution. After full-length synthesis of the peptides, Boc-aminobenzoic acid (Abz; Bachem, Bachem AG; Bubendorf, Switzerland) was coupled to the *N*-terminus of each hFF03 variant as a chromophore. Further synthesis of hFF03-variants was performed by selective deprotection of lysine(Mtt) side chain by treatment with a solution containing 1% TFA (v/v) and 1% MeOH (v/v) in DCM according to literature established protocols.[33] The free amine group of lysine 17 side chain is used as starting point for further coupling of either RGD or mannose.

In case of the tripeptide RGD, manual SPPS was performed using the respective amino acid (8 eq.), HATU (8 eq.) and DIPEA (16 eq.) relative to resin loading. Fmoc-deprotection was performed at each step as described above.

In case of mannose-functionalization, amino functionality was converted into a carboxy-functionality by addition of a mixture of glutaric anhydride (3 eq.) and catalytic amounts of DIPEA. The syringe was shaken for 3 h. Afterwards carboxy function was activated using (1-Cyano-2-ethoxy-2-oxoethylidenaminooxy)dimethylamino-morpholino-carbenium hexafluoro-phosphate (COMU, 3. eq.) and DIPEA (6 eq.). Immediately after, 1-amino-1-deoxy-mannopyranose (Santa Cruz) was coupled to carboxy function.

Full cleavage of all peptides from resin was performed by addition of 10 mL of a cleavage cocktail containing 95 % TFA, 3% H_2O and 2% Triisopropylsilane (TIS) to the corresponding syringe followed by 3.5 h of agitation. Peptides were precipitated using ice cold diethylether. After decantation of ether, peptides were redissolved in water and lyophilized. Purification of peptides was achieved using preparative HPLC.

Exchange of TFA adduct

TFA adducts inevitably obtained during full cleavage of peptides from resin using TFA and subsequent RP-HPLC purification using eluents containing 0.1% TFA, was exchanged against chloride according to established literature protocols.[34] Briefly, peptides were dissolved in water at a concentration of 0.52 mM. Afterwards 6 M HCl was mixed to peptide solutions to give final concentration of 7.5 mM HCl. The solutions were stirred at room temperature for 1 minute prior to lyophilization. This procedure was repeated 5 times.

Dialysis of peptides

Dialysis of peptides was performed by using Spectra/Por® Float-A-Lyzer® (Carl Roth) with molecular weight cut-off of 100-500 Da according to suppliers' instructions. Peptides were dialyzed against deionized water over three days. Water was changed three times a day. After completion, peptide solutions were lyophilized.

Sample preparation

Pure peptides were dissolved in 1 mL 1,1,1,3,3,3-Hexafluoroisopropanol (HFIP) and sonicated for 15 min. Peptide concentration was determined by UV-spectroscopy at 320 nm (Abz). An aliquot of the stock solution was briefly evaporated using a stream of N_2-gas and the pellet dissolved in 1 mL of D-PBS containing 6 M of guanidine hydrochloride. Absorbance at 320 nm

of this solution was measured using a Varian Cary 50 photometer (Varian Medical Systems, Palo Alto, CA, USA). The concentrations of stock solutions were calculated using a calibration curve of Abz-Gly-OH. For certain peptide concentrations, the required aliquots were completely evaporated and dissolved in buffer solution. In case of hydrogel-mixtures aliquots of desired peptide stock-solutions were mixed before evaporation. After evaporation, peptides were dissolved in dulbeccos phosphate buffered saline (Lonza, w/o Mg^{2+}, Ca^{2+}) or DMEM (Lonza, 4.5 g/L glucose). and pH adjusted to 7.4 using HCl or NaOH.

CD spectroscopy

CD spectra of peptide hydrogels were recorded using a Quartz Suprasil® cuvette with detachable windows and a path length of 0.1 mm (Hellma Analytics, Müllheim, Germany). Measurements were performed at 37 °C. A mean of three independent measurements was performed. CD spectra are background-corrected by subtraction of buffer spectra at 37 °C and spectra were normalized according to the path length of the cuvette, peptide concentration and number of amide-bonds.

Cryo-Transmission Electron Microscopy (cryo-TEM)

Cryo-TEM was measured using 0.15 wt% peptide hydrogel samples. 5 µl aliquots of the respective peptide gels were applied to pre-cleaned 200 mesh perforated carbon film-covered microscopical grids (R1/4 batch of Quantifoil, MicroTools GmbH, Jena, Germany). The grids were cleaned with chloroform and hydrophilized by 60 s glow discharging at 8 W in a BALTEC MED 020 device (Leica Microsystems, Wetzlar, Germany). Vitrifying of the samples occurred by automatic blotting and plunge freezing with a FEI Vitrobot Mark IV (Thermo Fisher Scientific Inc., Waltham, Massachusetts, USA) using liquid ethane as cryogen. The vitrified samples were transferred to the autoloader of a FEI TALOS ARCTICA electron microscope (Thermo Fisher Scientific Inc., Waltham, Massachusetts, USA). The microscope is equipped

with a high-brightness field-emission gun (XFEG), which operates at an acceleration voltage of 200 kV. Acquisition of the micrographs was carried out on a FEI Falcon 3 direct electron detector (Thermo Fisher Scientific Inc., Waltham, Massachusetts, USA) using a 70 µm objective aperture at a nominal magnification of 28,000 or 36,000 x, corresponding to a calibrated pixel size of 3.69 or 2.97 Å/pixel, respectively.

Rheology

All rheological measurements were performed using a temperature-controlled Bohlin Gemini 200 HR Nano rheometer using the strain-imposed mode. The samples were measured at room temperature (25 °C) and at physiological temperature (37 °C). All experiments were conducted using a plate-plate geometry with the upper rotating plate having a diameter of 40 mm. The plates are made of stainless steel. The gap size between the two plates was kept constant at 200 µm. To avoid evaporation effects the setup of sample and confining geometry was surrounded by a solvent trap. For reasons of reproducibility, all rheological experiments were repeated three times. From these triplicate measurements the error bars were estimated and found to be in the range of 10 to 20% of the measured values.

Small angle neutron scattering (SANS)

SANS experiments were performed at the Helmholtz-Zentrum Berlin (HZB, Berlin, Germany) on the instrument V4 and at the Laboratoire Leon Brillouin (LLB, Saclay, France) on the instrument PAXY. For the measurements at V4 (HZB) three different sample-detector-distances D_1 = 1.35 m, D_2 = 6.75 m and D_3 = 16.0 m were used. The wavelength for D_1 and D_2 was set at 4.5 Å, while for D_3 a wavelength of 10.0 Å was used. This enabled covering a q-range of 0.02 – 6.5 nm^{-1}, where $q = 4\pi \sin(\theta/2)/\lambda$ is the scattering vector with θ being the scattering angle. Also for the measurements at PAXY (LLB) three sample-detector-distances D_1 = 1 m, D_2 = 5 m, and D_3 = 6.7 m were used, whereby for D_1 and D_2 the wavelength was set

to 4.0 Å and for D_3 to 12.0 Å allowing to cover a q-range of 0.04 – 6.3 nm^{-1} similar to the experiments at V4. To have comparable experimental conditions for all measurements 2 mm Hellma QS 110 cuvettes were used throughout. During the experiments all samples were kept at 25 °C. To reduce the two-dimensional detector images to one-dimensional datasets the BerSANS software[35] was used for the data collected at V4, while for the data recorded at PAXY the PASiNET software[36] was used. For both reduction methods the one-dimensional data were obtained as differential cross sections by taking into account the samples transmission and comparing the scattering intensities to the one of a H_2O sample with 1 mm thickness.

Cytotoxicity of different hydrogel compositions

Cell Culture

NIH/3T3 embryonic mouse fibroblast cells were cultured in DMEM culture medium (Lonza, 4,5 g/L glucose, 10 % FCS, 1% penicillin/streptomycin) in a humidified incubator (5% CO_2, 37 °C). The cells were grown in 175 cm^2 cell culture flaks and medium was changed three times a week. Upon confluency of 70% - 80% the culture was subcultured according to the detected cell number.

Cytotoxicity assay of hydrogel cultured NIH/3T3 cells by use of Cell Counting Kit-8 (CCK-8)

To determine whether different peptide hydrogel compositions would be tolerated by the cells CCK-8 was used to conduct viability of cells during a 3 days cell culture. A suspension of NIH/3T3 cells in DMEM (4.5 g/L, 10% FCS, 1% penicillin/streptomycin) was seeded in a transparent 96-well plate with a density of 10.000 cells in an overall volume of 100 µL per well containing the respecting hydrogels. 10 µL of 1% (w/v) SDS was added to the respective wells of positive control and the plate was further incubated for 24 h and 72 h at 37 °C and 5% CO_2 respectively. After each time point 10 µL of CCK-8 solution was added to each well and

allowed to incubate for 2 h in a humidified incubator at 37 °C. During this time dehydrogenases in viable cells reduces WST-8 tetrazolium to formazan, which will be detected by measuring the absorbance at 450 nm. Absorbance was measured by using a Tecan Infinite 200 Pro microplate reader. Three experiments were performed in triplicates per hydrogel candidate (n=3).

Results and Discussion

ECM mimic design and preparation

The studied hFF03 and its variants originate from the fibril-forming homodimeric coiled coil peptide FF03, previously reported by our group.[13] It consists of 3.5 heptad repeats,[13] thus creating "sticky ends" at the *N*-terminus of the peptide to trigger fiber-assembly.[13,18] Leucine residues comprise the hydrophobic core (positions a and d) of the coiled-coil, whereas additional stabilization of the α-helical coiled-coil structure occurs by positively and negatively charged amino acids lysine and glutamic acid in positions e and g. Furthermore, b and c positions are occupied with alanine residues to shield the solvent-exposed domain of the peptide and induce weak hydrophobic interactions between helices, thus, promoting fiber formation.[30] Solvent-exposed position f of hFF03 is occupied by lysine to enable side-chain functionalization using amine chemistry. Instead of the commonly used Boc-protected lysine, a methyltrityl-protected (Mtt) lysine was placed in position 17 (Mtt). The Mtt-group can be selectively removed[33] to access the ε-NH_2 of lysine for functionalization or built-up of the RGD sequence, by orthogonal solid-phase peptide synthesis (SPPS). RGD sequence was chosen, as it is a well-known recognition motif that promotes adhesion of cells and is presented by fibronectin and collagen in native ECMs.[37,38]

For the conjugation with the carbohydrate ligand mannose, the ε-NH_2 of lysine 17 was converted into a carboxy-functionality by reaction with glutaric anhydride.[13] Activation of the

newly obtained carboxylic acid at the lysine side chain on resin and coupling of amino-functionalized mannose yields the corresponding peptide-carbohydrate conjugate. The monosaccharide mannose was chosen to study the impact of a sugar moieties on the hydrogel formation of the peptide. Based on this strategy (see Figure S1), a peptide library containing the undecorated peptide scaffold hFF03, a RGD-functionalized hFF03-K17-RGD, and a mannose-functionalized hFF03-K17-Man were synthesized (see Table 1).

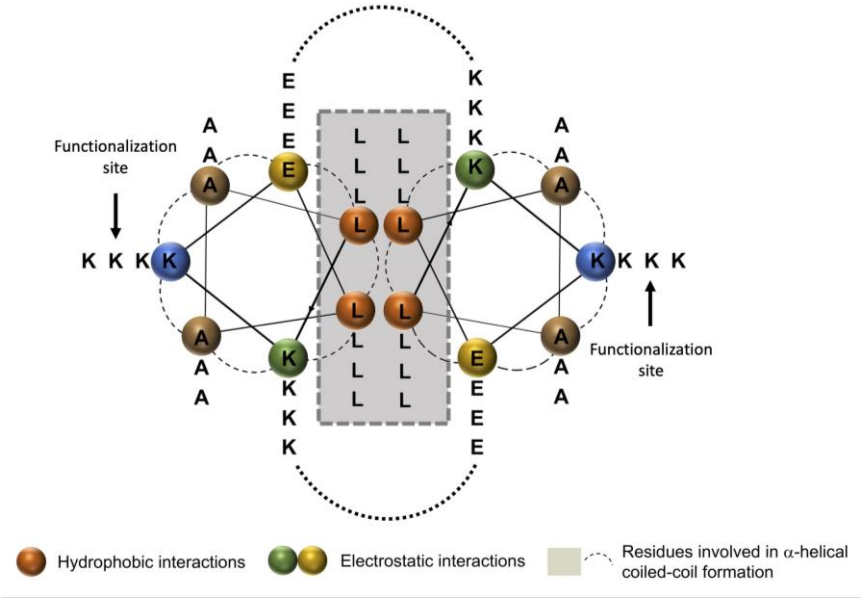

Figure 2. Helical wheel projection of peptide scaffold hFF03. Orange residues provide hydrophobic interaction, green and yellow residues provide electrostatic interaction. Remaining residues (brown and blue) are solvent exposed.[32]

Table 1. Synthesized peptide hFF03 and its modified variants. Bold K represents ligand bearing position.

	Sequence/Ligand
hFF03	LKKELAALKKELAALK**K**ELAALKKEL
hFF03-K17-Man	LKKELAALKKELAALK**K(Man)**ELAALKKEL
hFF03-K17-RGD	LKKELAALKKELAALK**K(RGD)**ELAALKKEL

Pure peptide hydrogels of hFF03 and its variants, and hydrogel mixtures were prepared and studied using overall peptide contents of 0.15 wt%, 0.30 wt%, and 0.50 wt% in order to systematically investigate the effect of increasing peptide concentration on properties of the respective hydrogels.

12 out of 18 compositions (see Table S) immediately formed self-supporting gels within an incubation time of 30 minutes. Initial hydrogel formation was tested by inverting the sample vials for 30 min at room temperature (inversion test). This simple test is commonly used to evaluate gel formation of peptides.[30,39] Inversion test was also performed at 37 °C and showed no melting effects for all peptide hydrogel mixtures. In addition, mixtures consisting of hFF03 and 1% of hFF03-K17-Man, hFF03 and 5% of hFF03-K17-RGD, and a combination of both (hFF03 + 1% hFF03-K17-Man + 5% hFF03-K17-RGD) were studied in terms of peptide structure and respective hydrogel formation. The latter mixture was chosen as this composition is close to the content of mannose and RGD in native ECMs.

Analysis of peptide structure and scaffold formation

Circular Dichroism

hFF03 and its functionalized variants and mixtures show CD-spectra characteristic for an α-helical secondary structure with typical ellipticity minima around 208 nm and 222 nm as well as an ellipticity maximum at 195 nm with minimal differences between the studied samples (see Figure 2). For all samples, the ellipticity minimum around 222 nm is of higher intensity than the minimum around 208 nm indicating the formation of higher ordered structures.[40] The intensities of CD spectra subsides in the order hFF03, hFF03 + 1% hFF03-K17-Man, hFF03 + 5% hFF03-K17-RGD, hFF03 + 1% hFF03-K17-Man + 5% hFF03-K17-RGD, hFF03-K17-Man, hFF03-K17-RGD, which indicates disturbed fiber formation due to the incorporation of

RGD and mannose ligands as was also previously discussed for modified variants of the peptide scaffold FF03.[13]

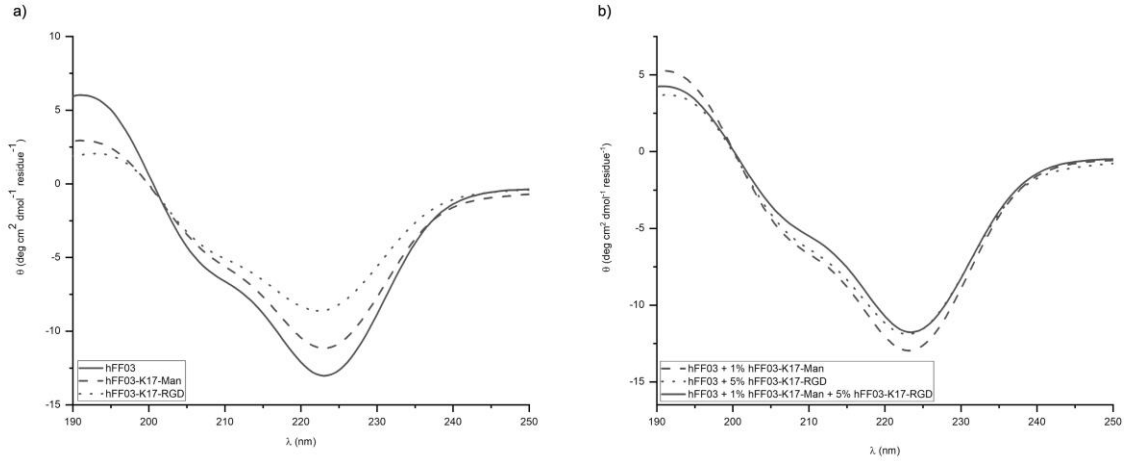

Figure 3. CD-spectra of 0.5 wt% peptide hydrogels directly after sample preparation at 37 °C. (a) pure peptide hydrogels, solid line – hFF03; dashes – hFF03-K17-Man; dottet – hFF03-K17-RGD (b) peptide hydrogel mixtures.

Cryo TEM

The morphology of the peptide hydrogels was determined at peptide contents of 0.15 wt%, as density of peptide fibers would otherwise be too high to obtain reasonable micrographs. Cryo-TEM micrographs show that all three hydrogels consist of a homogenous network of extended peptide fiber bundles with a diameter of 3 nm. Additionally, in the tested hydrogel mixture composed of hFF03 + 1% hFF03-K17-Man + 5% hFF03-K17-RGD vesicular inclusions are found within the network structure of the hydrogel. These inclusions might result from hetero-assembled peptide fibers as cryo-TEM of the pure functionalized peptide hydrogels hFF03-K17-Man and hFF03-K17-RGD showed no vesicular inclusions over their whole three-dimensional structure.

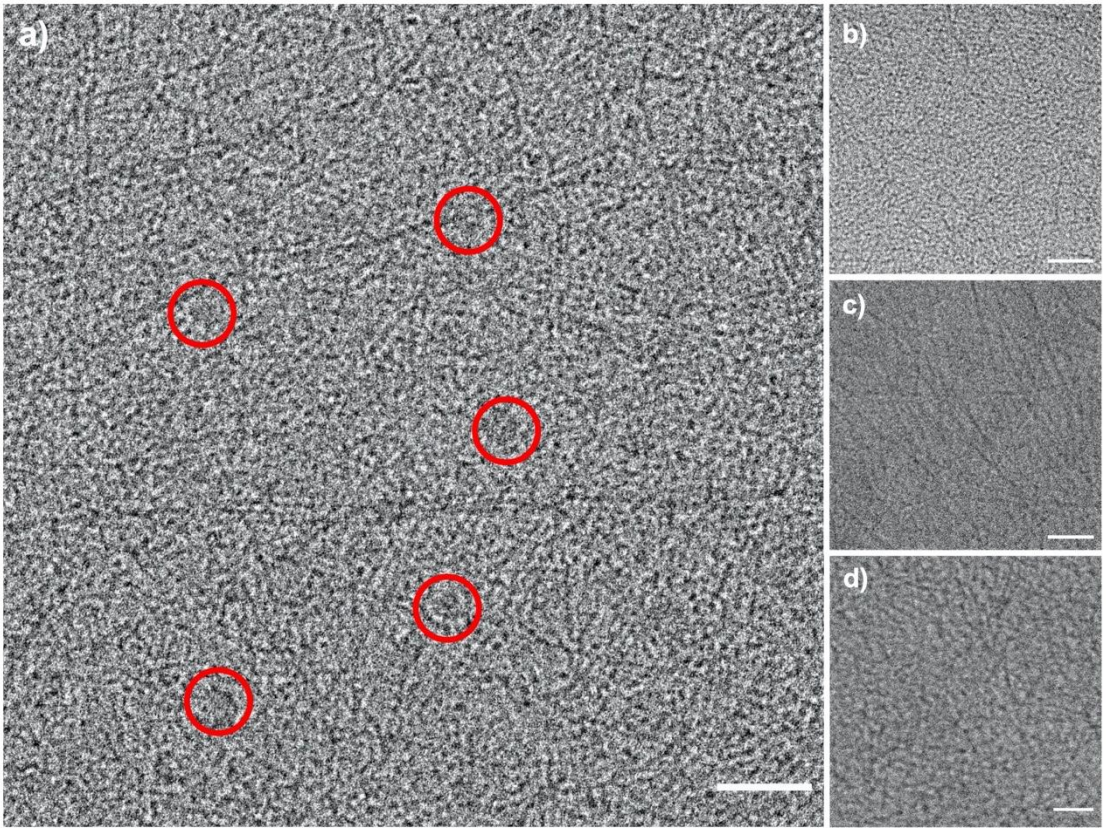

Figure 4. Cryo-TEM images of 0.15 wt% peptide hydrogels. (a) hFF03 + 1% hFF03-K17-Man + 5% hFF03-K17-RGD; (b) hFF03; (c) hFF03-K17-Man; (d) hFF03-K17-RGD. Vesicular inclusions are marked by red circles. The scale bar denotes 50 nm.

Rheological Characterization

In order to compare the stiffness, respectively the elastic and viscous properties of the hydrogels, which are the critical parameters within the context of biological or medical application, the pure peptide samples (with and without decoration by peptide or carbohydrate ligand) as well as mixtures thereof were investigated by shear strain oscillatory rheology. To ensure that the frequency dependent measurements are done within the linear viscoelastic (LVE) regime an amplitude sweep in the deformation mode was performed prior to each experiment (see **Erreur ! Source du renvoi introuvable.** and Table S1), yielding the amplitude

to be fixed at a deformation of 2% for all experiments. From the subsequent frequency sweeps in the range of 0.05 to 20 Hz it was possible to determine the storage and loss moduli, G' and G'', reflecting the elastic and viscous properties, respectively. The corresponding data sets for the hFF03 and decorated analogues are presented in Figure 5 (a) and (b) and the data for the mixed peptide systems are presented in Figure 5 (c) and (d).

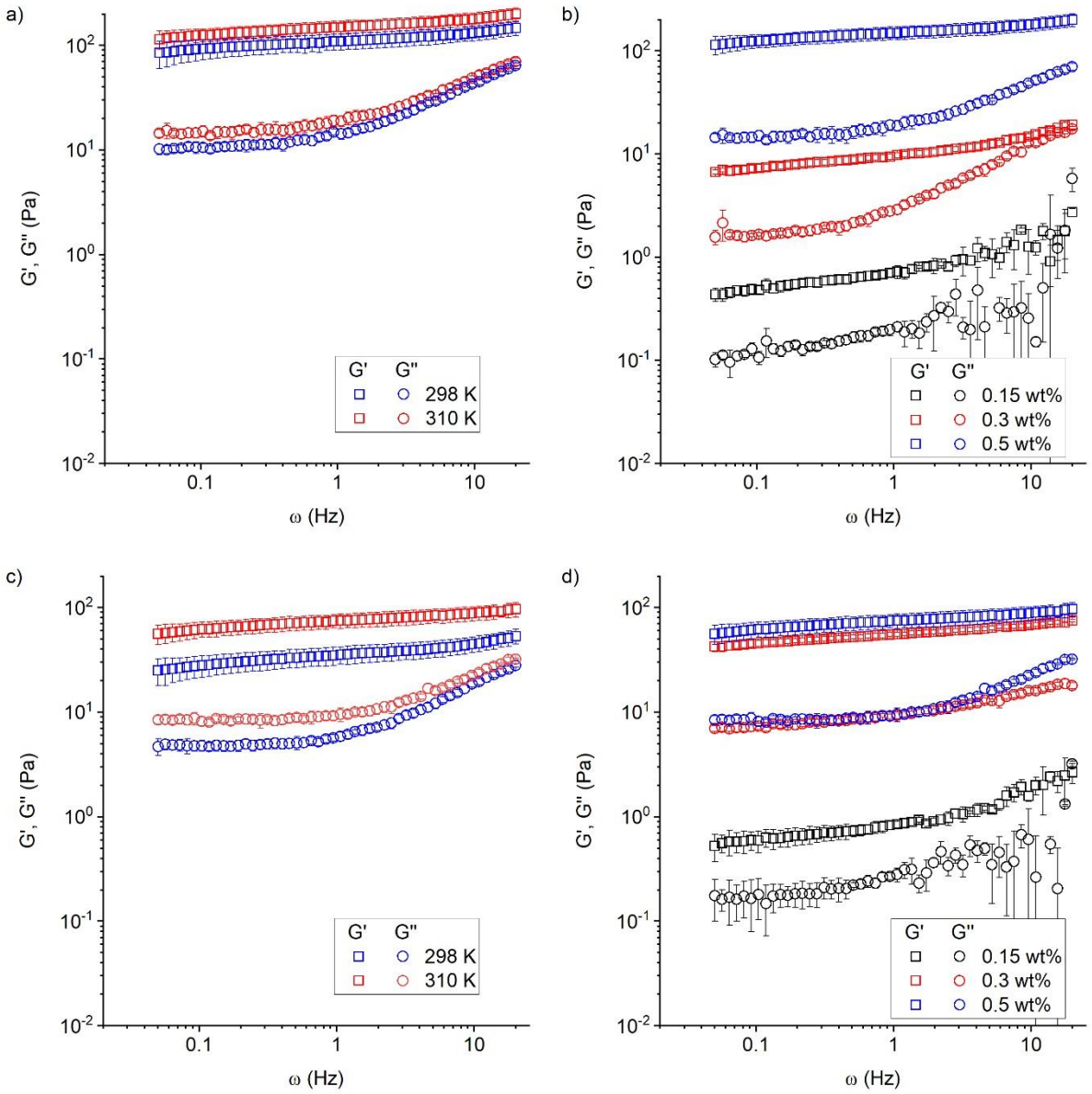

Figure 5. Moduli G' and G'' of hFF03 for (a) 25 and 37 °C at 0.5 wt%, and (b) at 37 °C for different concentrations, and analogous of hFF03 + 1% hFF03-K17-Man + 5% hFF03-K17-RGD for (c) 25 and 37 °C at 0.5 wt%, and (d) at 37 °C for different concentrations.

For all systems studied the elastic part, described by the G', is one decade larger than the viscous part, described by G'', and this difference becomes larger with increasing concentration and at low frequencies. Both moduli are rather constant, in general just increasing somewhat with frequency, and only G'' increases more strongly at higher frequency, indicating that here a mechanism for a more pronounced dissipation of mechanical energy becomes effective. The rather constant moduli indicate that in general these are gel-like systems. However, all samples are flowing very slowly (within 24 h) when turned upside down within their container, thereby demonstrating their finite structural relaxation time or at least a yield stress lower than that exerted by gravitation. A very interesting observation here is, that the elastic and viscous properties of the systems increase with rising temperature, whereas normally the opposite trend is observed. However, the strength of the gel in terms of the critical deformation that can be exerted to it is lower at higher temperature (Figure 5). This indicates that here complex mechanisms determining the mechanical properties must be present by which the moduli increase with increasing temperature, but this more elastic gel then can sustain only a smaller deformation, changes that must be related to molecular reorganizations as a function of temperature.

To further characterize the frequency-dependent properties of the system the phase angle δ(ω) (loss factor) defined as:

$$\tan\big(\delta(\omega)\big) = \frac{G''(\omega)}{G'(\omega)} \qquad \textbf{(1)}$$

is a good reference to classify the gels.

The phase angles of hFF03 and hFF03 + 1%hFF03-K17-Man +5%hFF03-K17-RGD are exemplarily shown in Figure 6 (a) and (b) for a temperature of 37 °C, which is the relevant temperature in the context of medical and biological applications (a comparison to data recorded at 25 °C is given in Figure S3). It is found that the phase angle is small for frequencies below 1 Hz, thereby quantifying the dominance of the elastic properties. Above 1 Hz it

increases with increasing frequency, showing that here then the viscous properties of the gels become more prominent. [41,42] Further, as a function of concentration a smaller phase angle is observed, which indicates more pronounced elastic properties at higher concentrations.

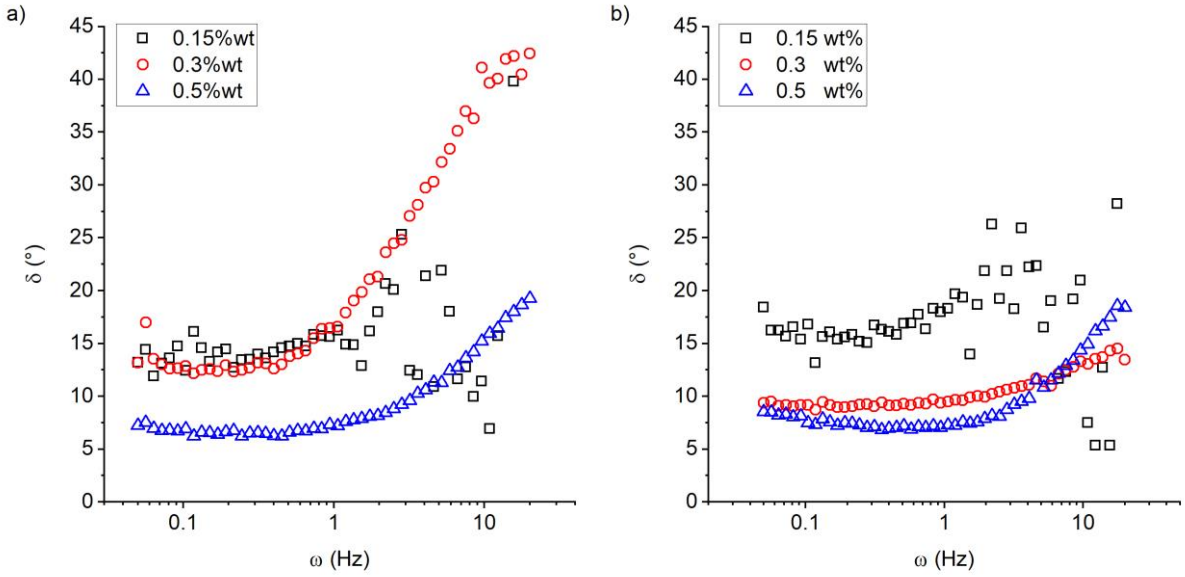

Figure 6. Phase angle at 37 °C of (a) hFF03 and (b) hFF03 + 1%hFF03-K17-Man + 5%hFF03-K17-RGD at different concentrations.

Usually, the Kelvin-Voigt model is a good candidate to describe the frequency dependent moduli G' and G'' of viscoelastic or gel-like materials, where the storage modulus G' is a constant (and related to the plateau modulus) and G'' is linearly depending on the frequency with the viscosity of the material being the corresponding proportionality constant.[42] However, for the system under investigation this approximation is not suitable to describe the data, because neither G' is really constant nor is G'' purely linearly depending on the frequency. Due to this fact, the so-called fractional Kelvin-Voigt model is employed. Within this model the moduli are described as follows

$$G'(\omega) = E\,\omega^{\alpha}\cos\left(\frac{\pi\,\alpha}{2}\right) + G_0$$

$$G''(\omega) = E\,\omega^{\alpha}\sin\left(\frac{\pi\,\alpha}{2}\right) \qquad \textbf{(2)}$$

Details for the derivation of these quantities are given elsewhere.[42,43] In Eq. (2) E is a fractional viscosity in units Pa s^{α} depending on the fractional exponent α ($0 < \alpha < 1$) and G_0 is the static load, equivalent to the plateau modulus (in the high frequency limit). Using this description, it is possible to model G' in an appropriate manner for the whole frequency range, while for G'' the approximation works only in the high frequency regime, which might be attributed to inertia effects at low frequencies. The static load G_0 can be used to given an estimate for the crosslinking number density N_C and the corresponding average mesh size ξ through[44]

$$N_C = \frac{G_0}{k\,T} = \frac{1}{\xi^3} \qquad \textbf{(3)}$$

Here, k is the Boltzmann constant and T is the absolute temperature. The results for ξ are tabulated in Tab. 2 for both investigated temperatures.

Table 2. Average mesh size ξ and static load G_0 as determined from fitting the data presented in Figure 5 (b) and (d) by the expressions for moduli given in Eq. (2), which are derived from the fractional Kelvin-Voigt model. The indices refer to the corresponding temperature T_1 = 25 °C and T_2 = 37 °C, respectively. The measurements have been carried out at 200 μm.

Name	c (wt%)	G_1 (Pa)	ξ_1 (nm)	G_2 (Pa)	ξ_2 (nm)
hFF03	0.15	0.29	242.0	0.45	211.7
	0.30	3.65	104.0	6.00	89.3
	0.50	95.20	35.1	57.24	42.1
hFF03-K17-Man	0.15	2.66	115.6	6.08	88.9
	0.30	0.94	163.8	4.32	99.7
	0.50	6.03	88.0	15.28	65.4
hFF03-K17-RGD	0.15	1.63	136.3	1.33	147.7
	0.30	8.78	77.7	15.15	65.6
	0.50	37.55	47.8	39.09	47.8
hFF03 + 1% hFF03-K17-Man	0.15	0.27	246.9	0.33	235.5
	0.30	8.23	79.3	20.17	59.6
	0.50	22.44	56.8	19.42	60.4
hFF03 + 5% hFF03-K17-RGD	0.15	1.67	135.2	2.39	121.4
	0.30	17.48	61.7	23.26	56.9
	0.50	24.21	55.4	32.11	51.1
hFF03 + 1%hFF03-K17-Man + 5%hFF03-K17-RGD	0.15	0.17	290.7	0.60	192.2
	0.30	16.97	62.3	16.61	63.6
	0.50	32.27	50.3	39.68	47.6

Comparing the values for the mesh size ξ presented in **Table 2**, it is found that in general ξ is decreasing with increasing concentration c. This is expected, however for simple rod-like fibers one would expect a scaling of $\xi \sim c^{-0.5}$, while here the experimental changes are much larger. This indicates that the effective strengthening of the polypeptide works in a much more

effective way than by the simple increase of overlapping junctions of the polymer chains. Further, it is notable that the mesh sizes at both temperatures, 25 °C and 37 °C, are of the same order of magnitude and follow the same trends.

Small Angle Neutron Scattering (SANS)

In order to get a more detailed insight into the structural organization of hFF03 and its decorated analogues (hFF03-K17-Man and hFF03-K17-RGD) on a mesoscopic level, SANS measurements were performed for different peptide concentrations (0.15, 0.3 and 0.5 wt%). Further, mixtures of the pure and the decorated peptides were investigated. The scattering patterns for hFF03 without decoration and hFF03 + 1%hFF03-K17-Man + 5%hFF03-K17-RGD as function of the concentration are shown in Figure 7 (a) and (b), respectively.

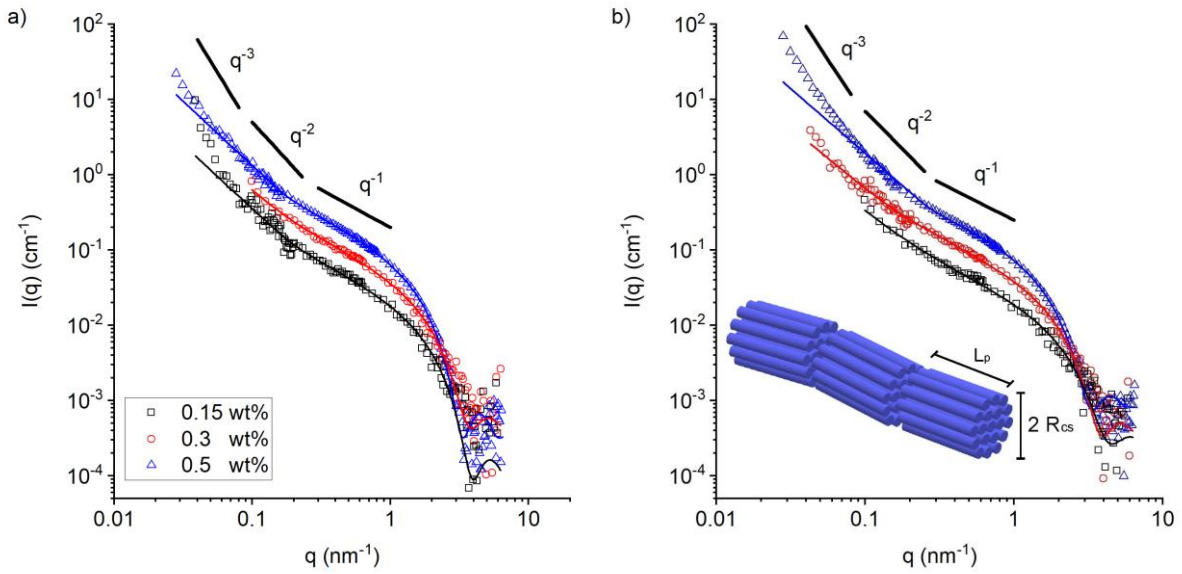

Figure 7. Scattering patterns of (a) hFF03 and (b) hFF03 + 1%hFF03-K17-Man + 5%hFF03-K17-RGD at different concentrations. The solid lines represent fits with a form factor model for flexible cylinders as suggested by Pedersen and Schurtenberger.[45] The temperature for all experiments was kept at 25 °C.

Comparing the intensities of the scattering data presented in Figure 7, a well-defined concentration trend can be observed. That is, the intensity is increasing with increasing concentration for the investigated q-range. A direct comparison of scattering intensities of peptide hydrogels grouped by the three concentrations as shown in Figures S9 and S10 yields no difference between pure and decorated peptides. Hence, in the range of 1-50 nm their overall network structure must be very similar.

For all scattering patterns at intermediate q values an intensity scaling of q^{-1} can be taken as an indication for the formation of local rod-like structures[45]. In the lower q range the slope then increases substantially, following a power law of ~ q^{-3} at lowest q, a behavior quite typically seen for the network structure of hydrogels.[46,47] The cross-over between the two power laws is indicative of the length of the local rod-like structure of the peptide chains. Such a structural arrangement is usually characterized by the persistence length L_p and the cross-sectional radius R_{cs}. In order to determine the latter one, the scattering data in the intermediate q regime were approximated by a modified Guinier approximation,[48,49] given by

$$I(q) = \frac{A}{q} \cdot \exp\left(-\frac{q^2 R_{g,m}^2}{2}\right) \text{ with } R_{g,m}^2 = \frac{R_{cs}^2}{2}. \quad \textbf{(4)}$$

In Eq. (4) the pre-factor A on the right-hand side of the equation denotes the forward scattering intensity per unit length. R_{cs} is always in the range of 0.7-1.3 nm^{-1} (Table 3) and reflects the effective thickness of a bundle of peptide chains. The quantitative analysis described in the SI shows that these bundles correspond to 10-20 peptide chains (N_{pep}, Table S4). R_{cs} is generally decreasing with increasing concentration, which signifies that the chains are more stretched for the more dilute case, something to be expected in order to form a space-filling network. Comparing the cross-sectional radii obtained from fitting the intermediate q regime with Eq. (4) the values are in good agreement with the results from TEM as presented in Figure 4 .

Table 3. Fit results for the cross-sectional radius R_{cs} obtained from applying Eq. (4) to the scattering data, and for persistence length and cross-sectional radius obtained by fitting the data with the Pedersen-Schurtenberger model for flexible, rod-like structures.[45]

Name	*c* (wt%)	R_{cs} (nm)	L_p (nm)	R_{cs} (nm)
hFF03	0.5	1.30	9.81	1.14
	0.3	1.04	13.54	0.99
	0.15	1.01	9.20	0.96
hFF03-K17-Man	0.5	1.24	7.49	1.18
	0.3	1.18	8.94	1.09
	0.15	1.05	8.42	1.01
hFF03-K17-RGD	0.5	1.11	8.95	1.02
	0.3	1.30	9.96	1.09
	0.15	0.74	10.41	1.01
hFF03 + 1% hFF03-K17-Man	0.5	1.16	9.10	1.14
	0.3	0.78	12.68	0.79
	0.15	0.94	10.44	0.86
hFF03 + 5% hFF03-K17-RGD	0.5	1.16	6.96	1.14
	0.3	0.99	14.15	0.96
	0.15	1.03	9.80	0.98
hFF03 + 1% hFF03-K17-Man + 5% hFF03-K17-RGD	0.5	1.16	6.59	1.14
	0.3	1.03	12.27	0.97
	0.15	0.91	10.70	0.84

For a more accurate description of the scattering data, the intensities are approximated by a form factor model based on the flexible cylinder model as implemented in SasView.[50] This model originates from simulations done by Pedersen and Schurtenberger on semiflexible polymers, which take into account, excluded volume effects.[45] The scattering length density of the peptides is assumed to be $3.0 \cdot 10^{10}$ cm^{-2}.[51] Comparing the cross-sectional radii obtained

from the modified Guinier approximation and the Pedersen-Schurtenberger model, they are found to be in good agreement. Further, it is notable that the persistence length of the peptides is for all samples in the same order of magnitude and is around 8-14 nm. Assuming the peptide chains to be fully stretched they are found to be on average 17.2 nm, which is in good agreement with the determined persistence length. Further, the persistence length is also determined from a Kratky-plot (see exemplary Fig. S5) yielding values around 15 nm (Table S3) and therefore confirming this observation. This means that the peptide chains are rather stretched and cylindrical in these network structures.

Cytotoxicity of peptide hydrogels

hFF03 and its variants were studied as 3D-cell culture substrates and their cytotoxicity was assessed. To enhance biocompatibility of the studied peptides TFA counterions, inevitably added during peptide resin cleavage and subsequent purification by HPLC (eluents containing 0.1% TFA), were exchanged for chloride ions by treatment of the respective peptides with diluted HCl according to established protocols.[34]

Various hydrogel candidates were studied in a three-day cell culture by culturing embryonic mouse fibroblast cell line NIH/3T3 on hydrogel candidates, to assess optimal peptide content and compositions for cell growth (Figure 8). Cytotoxicity was determined relative to control standards, including pure medium, Matrigel® and SDS. The commercially available and commonly used 3D cell culture scaffold Matrigel®, which represents a mixture of different ECM proteins of the Engelbreth-Holm-Swarm mouse sarcoma, was used as negative control to compare viability of seeded cells on a 3D substrate. SDS was used to establish controlled cell death as positive control.

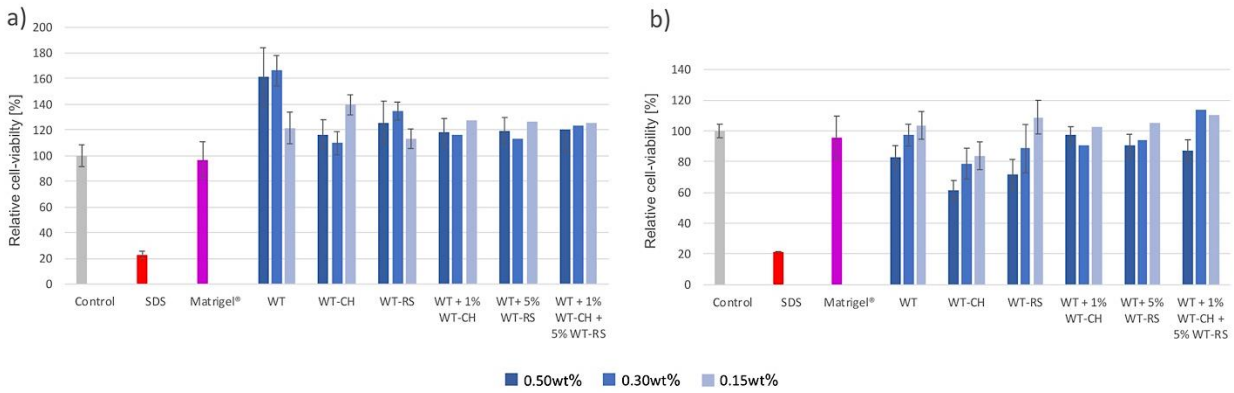

Figure 8. Viability profiles of seeded NIH3T3-cells on peptide hydrogels after a) 24h and b) 72h. WT: hFF03, WT-CH: hFF03-K17-Man, WT-RS: hFF03-K17-RGD.

An increased viability of seeded cells was observed for all tested hydrogels candidates after 24 h (Figure 8a). Compared to both controls (Medium and SDS), NIH/3T3 cells cultured on peptide hydrogels show a generally increased viability after 24 h. Especially the undecorated hFF03 hydrogel at 0.3 wt% was tolerated most by the cells resulting in viability values higher than 160%, compared to the control. Cells cultured on each peptide hydrogel mixture showed viabilities in the same range with variations up to 10%. After 72 h, relative cell-viability of cells cultured on 0.5 wt% hFF03-K17-Man hydrogels decreased to 60% (Figure 8b). Whereas the other two hydrogels containing 0.5 wt% peptide show profiles ranging from 70% to 97 % relative viability compared to the control. Also, for all 0.3 wt% hydrogels average viabilities between 94% and 78% were determined after 72 h. Strikingly, except for hFF03-K17-Man, all 0.15 wt% candidates show cell-viability profiles above 100% relative to both controls. The results show, on the one hand, that the newly designed coiled-coil-based peptide hydrogels are suitable cell-culture matrices; and on the other hand, that only small differences in matrix composition with regard to peptide content and presented ligand density have a great effect on cell-viability. Fine-tuning these parameters, and thus overall chemical and physical properties of the resulting hydrogels, presents a pivotal point in the design of artificial ECM. Within the presented system fine-tuning is readily performed by varying the concentrations of

functionalized coiled-coil monomers peptides. Hence, the presented approach enables an efficient methodology to access tailored biomaterials for the applications in cell culture experiments with optimized composition.

Conclusion

Herein, we report the development of a homomeric coiled coil-based peptide (hFF03) that forms self-supporting hydrogels and functions as a potent cell-culture matrix. Using an all-on-solid-phase-synthesis approach, hFF03 was functionalized with peptide sequence RGD or carbohydrate mannose to include biologically relevant ligands. Utilizing the modularity of the coiled-coil design, hFF03 and its functionalized variants were mixed to obtain hydrogels that comprise defined ratios of RGD or mannose ligands that are distributed and multivalently presented throughout the 3D-structure of the hydrogel. This approach allows for fine-tuning of concentration of functional ligands, thus, fine-tuning of physicochemical properties of the resulting artificial ECM. These new 3D constructs were studied regarding their structural and mechanical properties as well as cytotoxicity. Cryo-TEM and neutron scattering experiments revealed fibrillar networks with rather stiff and stretched fibrillar chains, characterized by persistence lengths of 10-15 nm and they are composed of about 10-20 parallel peptide chains. Oscillatory rheology showed that these networks respond mainly elastic and the storage modulus increases very strongly with rising peptide concentration. Interestingly, the elastic properties do not decrease with increasing temperature but even become somewhat larger. Initial cytotoxicity assays using NIH/3T3 cells showed an improved viability of seeded cell populations on hFF03-based peptide hydrogels. Compared to other *ex vivo* materials, the herein presented system has the advantage of being easily accessible by chemical synthesis, without significant batch-to-batch variation. Moreover, the herein described methodology enables the development of peptide hydrogels that are tunable with regard to composition and density of presented ligands, which are important factors in systematic approaches that correlate hydrogel

nature and properties with directing cellular behavior like proliferation and differentiation. Further studies on possible applications of the here described 3D materials in tissue engineering and stem cell differentiation are in progress.

AUTHOR INFORMATION

Corresponding Author

*Prof. Dr. Beate Koksch, Institute of Chemistry and Biochemistry – Organic Chemistry, Freie Universität Berlin, Takustraße 3, 14195 Berlin (Germany), Beate.Koksch@fu-berlin.de

Author Contributions

The manuscript was written through contributions of all authors. All authors have given approval to the final version of the manuscript. ‡These authors contributed equally.

Funding Sources

The project was funded by the DFG-CRC 765 Multivalency (SFB 765/2-2014).

ACKNOWLEDGMENT

The authors acknowledge financial support by the DFG-CRC 765 “Multivalency” (SFB 765/2-2014). Further, the authors thank the Laboratoire Léon Brillouin (Saclay, France) as well as the Helmholtz Zentrum Berlin (Berlin, Germany) for granting the neutron scattering beamtime at PAXY respectively V4 spectrometer.

ABBREVIATIONS

CCR2, CC chemokine receptor 2; CCL2, CC chemokine ligand 2; CCR5, CC chemokine receptor 5; TLC, thin layer chromatography.

BRIEFS (Word Style “BH_Briefs”). If you are submitting your paper to a journal that requires a brief, provide a one-sentence synopsis for inclusion in the Table of Contents.

SYNOPSIS (Word Style “SN_Synopsis_TOC”). If you are submitting your paper to a journal that requires a synopsis, see the journal’s Instructions for Authors for details.

REFERENCES

1. Hughes CS, Postovit LM, Lajoie GA. Matrigel: A Complex Protein Mixture Required for Optimal Growth of Cell Culture. *Proteomics* 2010;10(9):1886–1890, DOI: 10.1002/pmic.200900758.

2. Lin C., Bissell MJ. Multi-Faceted Regulation of Cell Differentiation by Extracellular Matrix. *FASEB J* 1993;7(9):737–743.

3. Martin GR, Kleinman HK. Extracellular Matrix Proteins Give New Life to Cell Culture. *Hepatology* 1981;1(3):264–266, DOI: 10.1002/hep.1840010312.

4. Kleinman HK, Graf J, Iwamoto Y, Kitten GT, Ogel RC, Sasaki M, Yamada Y, Martin GR, Luckenbill-Edds L. Role of Basement Membranes in Cell Differentiation. *Ann N Y Acad Sci* 1987;513(1):134–145, DOI: 10.1111/j.1749-6632.1987.tb25004.x.

5. Kleinman HK, Klebe RJ, Martin GR. Role of Collagenous Matrices in the Adhesion and Growth of Cells. *J Cell Biol* 1981;88(3):473–485, DOI: 10.1083/jcb.88.3.473.

6. Geckil H, Xu F, Zhang X, Moon S, Demirci U. Engineering Hydrogels as Extracellular Matrix Mimics.Geckil, H., Xu, F., Zhang, X., Moon, S., & Demirci, U. (2010). Engineering Hydrogels as Extracellular Matrix Mimics. Nanomedicine (London,

England), 5(3), 469–84. Http://Doi.Org/10.2217/Nnm.10.12. *Nanomedicine (Lond)* 2010;5(3):469–484, DOI: 10.2217/nnm.10.12.

7. Blow N. Cell Culture: Building a Better Matrix. *Nat Methods* 2009;6(8):619–622, DOI: 10.1038/nmeth0809-619.

8. Kleinman HK, McGarvey ML, Liotta LA, Robey PG, Tryggvason K, Martin GR. Isolation and Characterization of Type IV Procollagen, Laminin, and Heparan Sulfate Proteoglycan from the EHS Sarcoma. *Biochemistry* 1982;21(24):6188–6193, DOI: 10.1021/bi00267a025.

9. Kleinman HK, Martin GR. Matrigel: Basement Membrane Matrix with Biological Activity. *Semin Cancer Biol* 2005;15(5 SPEC. ISS.):378–386, DOI: 10.1016/j.semcancer.2005.05.004.

10. Tibbitt MW, Anseth KS. Hydrogels as Extracellular Matrix Mimics for 3D Cell Culture. *Biotechnol Bioeng* 2009;103(4):655–663, DOI: 10.1002/bit.22361.

11. Nguyen EH, Daly WT, Le NNT, Farnoodian M, Belair DG, Schwartz MP, Lebakken CS, Ananiev GE, Saghiri MA, Knudsen TB, Sheibani N, Murphy WL. Versatile Synthetic Alternatives to Matrigel for Vascular Toxicity Screening and Stem Cell Expansion. *Nat Biomed Eng* 2017;1(7):96, DOI: 10.1038/s41551-017-0096.

12. Lou S, Wang X, Yu Z, Shi L. Peptide Tectonics: Encoded Structural Complementarity Dictates Programmable Self-Assembly. *Adv Sci* 2019;1802043, DOI: 10.1002/advs.201802043.

13. Zacco E, Anish C, Martin CE, v. Berlepsch H, Brandenburg E, Seeberger PH, Koksch B. A Self-Assembling Peptide Scaffold for the Multivalent Presentation of Antigens. *Biomacromolecules* 2015;16(7):2188–2197, DOI: 10.1021/acs.biomac.5b00572.

14. Zacco E, Hütter J, Heier JL, Mortier J, Seeberger PH, Lepenies B, Koksch B. Tailored Presentation of Carbohydrates on a Coiled Coil-Based Scaffold for Asialoglycoprotein Receptor Targeting. *ACS Chem Biol* 2015;10(9):2065–2072, DOI: 10.1021/acschembio.5b00435.

15. Hellmund KS, Koksch B. Self-Assembling Peptides as Extracellular Matrix Mimics to Influence Stem Cell's Fate. *Front Chem* 2019;7:172, DOI: 10.3389/fchem.2019.00172.

16. Woolfson DN. The Design of Coiled-Coil Structures and Assemblies. *Adv Protein Chem* 2005;70(04):79–112, DOI: 10.1016/S0065-3233(05)70004-8.

17. Falenski JA, Gerling UIM, Koksch B. Multiple Glycosylation of de Novo Designed α-Helical Coiled Coil Peptides. *Bioorg Med Chem* 2010;18(11):3703–3706, DOI: 10.1016/j.bmc.2010.03.061.

18. Pagel K, Koksch B. Following Polypeptide Folding and Assembly with Conformational Switches. *Curr Opin Chem Biol* 2008;12(6):730–739, DOI: 10.1016/j.cbpa.2008.09.005.

19. Pagel K, Wagner SC, Araghi RR, Von Berlepsch H, Böttcher C, Koksch B. Intramolecular Charge Interactions as a Tool to Control the Coiled-Coil-to-Amyloid Transformation. *Chem - A Eur J* 2008;14(36):11442–11451, DOI: 10.1002/chem.200801206.

20. Lupas AN, Gruber M. The Structure of α-Helical Coiled Coils. In *Adv. Protein. Chem.*, Vol. 70. 2005; 37–38, DOI: 10.1016/S0065-3233(05)70003-6.

21. Hodges RS. De Novo Design of α-Helical Proteins: Basic Research to Medical Applications. *Biochem Cell Biol* 1996;74(2):133–154, DOI: 10.1139/o96-015.

22. Litowski JR, Hodges RS. Designing Heterodimeric Two-Stranded Alpha-Helical Coiled-Coils. *J Biol Chem* 2002;277(40):37272–37279, DOI: 10.1074/jbc.M204257200.

23. Harbury PB, Zhang T, Kim PS, Alber T. A Switch between Two-, Three-, and Four-Stranded Coiled Coils in GCN4 Leucine Zipper Mutants. *Science (80-)* 1993;262(5138):1401–1407, DOI: 10.1126/science.8248779.

24. Fletcher JM, Boyle AL, Bruning M, Bartlett SgJ, Vincent TL, Zaccai NR, Armstrong CT, Bromley EHC, Booth PJ, Brady RL, Thomson AR, Woolfson DN. A Basis Set of de Novo Coiled-Coil Peptide Oligomers for Rational Protein Design and Synthetic Biology. *ACS Synth Biol* 2012;1(6):240–250, DOI: 10.1021/sb300028q.

25. Wolf E, Kim PS, Berger B. MultiCoil: A Program for Predicting Two-and Three-Stranded Coiled Coils. *Protein Sci* 1997;6(6):1179–1189, DOI: 10.1002/pro.5560060606.

26. Banwell EF, Abelardo ES, Adams DJ, Birchall M a, Corrigan A, Donald AM, Kirkland M, Serpell LC, Butler MF, Woolfson DN. Rational Design and Application of Responsive Alpha-Helical Peptide Hydrogels. *Nat Mater* 2009;8(7):596–600, DOI: 10.1038/nmat2479.

27. Mehrban N, Abelardo E, Wasmuth A, Hudson KL, Mullen LM, Thomson AR, Birchall MA, Woolfson DN. Assessing Cellular Response to Functionalized α-Helical Peptide Hydrogels. *Adv Healthc Mater* 2014;3(9):1387–1391, DOI: 10.1002/adhm.201400065.

28. Mehrban N, Zhu B, Tamagnini F, Young FI, Wasmuth A, Hudson KL, Thomson AR, Birchall MA, Randall AD, Song B, Woolfson DN. Functionalized α-Helical Peptide Hydrogels for Neural Tissue Engineering. *ACS Biomater Sci Eng* 2015;1(6):431–439, DOI: 10.1021/acsbiomaterials.5b00051.

29. Potekhin SA, Melnik TN, Popov V, Lanina NF, Vazina AA, Rigler P, Verdini AS, Corradin G, Kajava A V. De Novo Design of Fibrils Made of Short α-Helical Coiled Coil Peptides. *Chem Biol* 2001;8(11):1025–1032, DOI: 10.1016/S1074-5521(01)00073-

4.

30. Banwell EF, Abelardo ES, Adams DJ, Birchall M a, Corrigan A, Donald AM, Kirkland M, Serpell LC, Butler MF, Woolfson DN. Rational Design and Application of Responsive α-Helical Peptide Hydrogels. *Nat Mater* 2009;8(7):596–600, DOI: 10.1038/nmat2479.

31. Pierschbacher MD, Ruoslahti E. Variants of the Cell Recognition Site of Fibronectin That Retain Attachment-Promoting Activity. *Proc Natl Acad Sci U S A* 1984;81(19 I):5985–5988, DOI: 10.1073/pnas.81.19.5985.

32. Hellmund KS. Coiled-Coil Based 3D Scaffolds as Highly Specialized Biological Microenvironments, Freie Universität Berlin, 2019.

33. MILLIPORE M. *Novabiochem (R) Guide to Selection of Building Blocks*.

34. Andrushchenko V V, Vogel HJ, Prenner EJ. Optimization of the Hydrochloric Acid Concentration Used for Trifluoroacetate Removal from Synthetic Peptides. *J Pept Sci* 2007;13(1):37–43, DOI: 10.1002/psc.793.

35. Keiderling U. The New "BerSANS-PC" Software for Reduction and Treatment of Small Angle Neutron Scattering Data. *Appl Phys A Mater Sci Process* 2002;74(SUPPL.II):1455–1457, DOI: 10.1007/s003390201561.

36. Brûlet A, Lairez D, Lapp A, Cotton J-P. Improvement of Data Treatment in Small-Angle Neutron Scattering. *J Appl Crystallogr* 2007;40(1):165–177, DOI: 10.1107/S0021889806051442.

37. Ruoslahti E. RGD and Other Recognition Sequences For Integrins. *Annu Rev Cell Dev Biol* 1996;12(1):697–715, DOI: 10.1146/annurev.cellbio.12.1.697.

38. Cha C, Liechty WB, Khademhosseini A, Peppas NA. Designing Biomaterials to Direct

Stem Cell Fate. *ACS Nano* 2012;6(11):9353–9358, DOI: 10.1021/nn304773b.

39. Lian M, Chen X, Lu Y, Yang W. Self-Assembled Peptide Hydrogel as a Smart Biointerface for Enzyme-Based Electrochemical Biosensing and Cell Monitoring. *ACS Appl Mater Interfaces* 2016;8(38):25036–25042, DOI: 10.1021/acsami.6b05409.

40. Pandya MJ, Spooner GM, Sunde M, Thorpe JR, Rodger A, Woolfson DN. Sticky-End Assembly of a Designed Peptide Fiber Provides Insight into Protein. *Biochemistry* 2000;39(30):8728–8734, DOI: 10.1021/bi000246g.

41. Bagley RL, Torvik PJ. Fractional Calculus—A Different Approach to the Analysis of Viscoelastically Damped Structures. *AIAA J* 1983;21(5):741–748, DOI: 10.2514/3.8142.

42. Eldred LB, Baker WP, Palazotto AN. Kelvin-Voigt versus Fractional Derivative Model as Constitutive Relations for Viscoelastic Materials. *AIAA J* 1995;33(3):547–550, DOI: 10.2514/3.12471.

43. Lewandowski R, Chorazyczewski B. Identification of the Parameters of the Kelvin-Voigt and the Maxwell Fractional Models, Used to Modeling of Viscoelastic Dampers. *Comput Struct* 2010;88(1–2):1–17, DOI: 10.1016/j.compstruc.2009.09.001.

44. Doi M, Edwards SF. *The Theory of Polymer Dynamics*. Oxford University Press, 1986.

45. Pedersen JS, Schurtenberger P. Scattering Functions of Semiflexible Polymers with and without Excluded Volume Effects. *Macromolecules* 1996;29(23):7602–7612, DOI: 10.1021/ma9607630.

46. Horkay F, Basser PJ, Hecht A-M, Geissler E. Structural Investigations of a Neutralized Polyelectrolyte Gel and an Associating Neutral Hydrogel. *Polymer (Guildf)* 2005;46(12):4242–4247, DOI: 10.1016/j.polymer.2005.02.054.

47. Vamvakaki M, Patrickios CS, Lindner P, Gradzielski M. Amphiphilic Networks Based

on Cross-Linked Star Polymers: A Small-Angle Neutron Scattering Study. *Langmuir* 2007;23(21):10433–10437, DOI: 10.1021/la700933p.

48. Hjelm RP, Thiyagarajan P, Alkan-Onyuksel H. Organization of Phosphatidylcholine and Bile Salt in Rodlike Mixed Micelles. *J Phys Chem* 1992;96(21):8653–8661, DOI: 10.1021/j100200a080.

49. Hjelm RP, Schteingart C, Hoffmann AF, Sivia DS. Form and Structure of Self-Assembling Particles in Monoolein-Bile Salt Mixtures. *J Phys Chem* 1995;99(44):16395–16406, DOI: 10.1021/j100044a030.

50. https://www.sasview.org/publications/.

51. Jacrot B. The Study of Biological Structures by Neutron Scattering from Solution. *Reports Prog Phys* 1976;39(10):911–953, DOI: 10.1088/0034-4885/39/10/001.

Supporting Information

Functionalized peptide hydrogels as tunable extracellular matrix mimics for biological applications

Katharina S. Hellmund[a], Benjamin von Lospichl[b], Christoph Böttcher[c], Kai Ludiwg[c], Uwe Keiderling[d], Laurence Noirez[e], Annika Weiß[a], Michael Gradzielski[b] and Beate Koksch[a]

[a] Institute of Chemistry and Biochemistry – Organic Chemistry, Freie Universität Berlin, Takustraße 3, 14195 Berlin (Germany)

[b] Stranski-Laboratory of Physical and Theoretical Chemistry, Institute of Chemistry, Technische Universität Berlin, Straße des 17. Juni 124, 10623 Berlin (Germany)

[c] Institute of Chemistry and Biochemistry and CoreFacility BioSupraMol Freie Universität Berlin, Fabeckstrasse 36a, 14195 Berlin (Germany)

[d] Helmholtz-Zentrum Berlin für Materialien und Energie, Hahn-Meitner-Platz 1, 14109 Berlin (Germany)

[e] Laboratoire Léon Brillouin (CEA-CNRS), CE-Saclay, 91190 Gif-sur-Yvette Cédex (France)

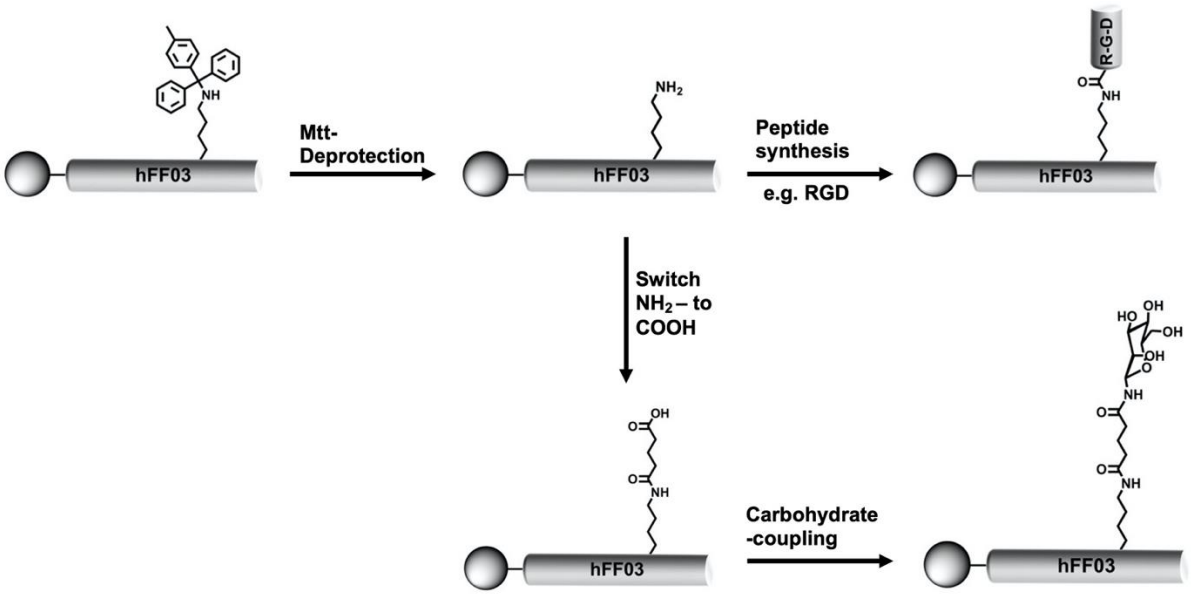

Figure S1. All-on-solid-phase synthesis scheme[32] of decorated hFF03 variants hFF03-K17-.

For the rheological characterization of the peptide hydrogel samples amplitude sweeps are performed prior to each experiment. Hereby, the frequency is fixed to 1 Hz and the amplitude expressed through the deformation γ of the sample is varied. The measurements are carried out at 25 °C and 37 °C. To derive the critical deformation γ*, that is the deformation limiting the linear viscoelastic (LVE) regime, two regions are assumed: For $\gamma < \gamma^*$, the data exhibit a plateau region, while for $\gamma > \gamma^*$ the data are decaying linearly. To distinguish both regions the data are plotted as log10(G') respectively log10(G'') vs. log10(γ) as shown in Figure S2 (a). The critical deformation γ* is determined from the intersection point of both linear regions. The results are summarized in Table S1.

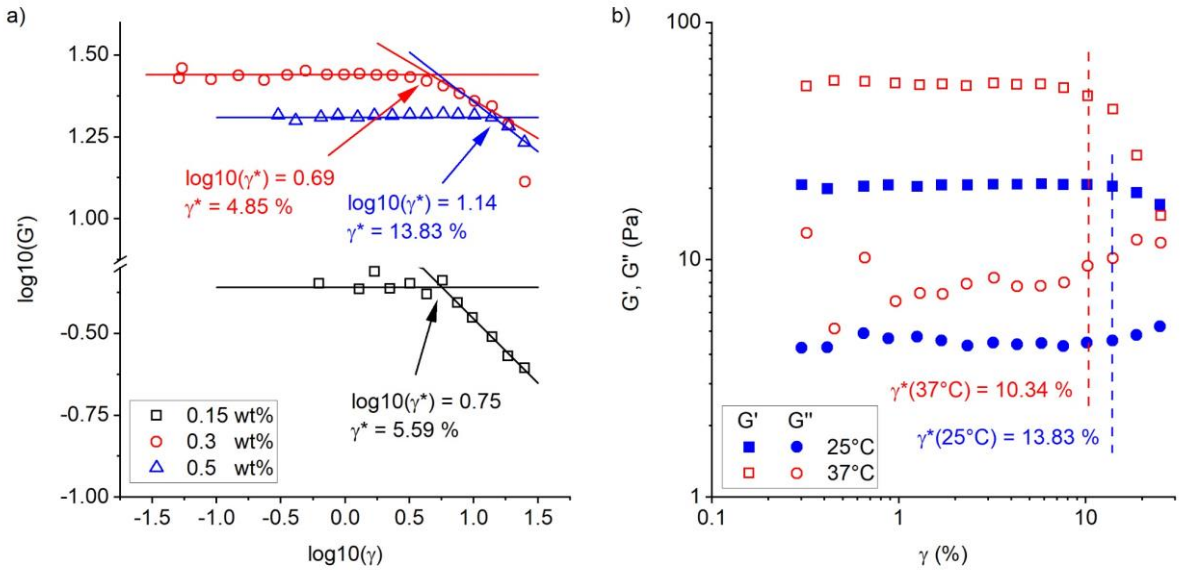

Figure S2. Amplitude sweep of hFF03 + 1% hFF03-K17-Man + 5% hFF03-K17-RGD at ω = 1 Hz for (a) different concentrations and 25 °C and (b) for different temperatures and c = 0.5 wt%. Solid lines in (a) are linear fits, the critical deformation γ* is determined from their intersection point. In (b) to dashed vertical lines indicate the position of γ*.

Comparing the values shown in Table S1, not clear trend is observed throughout all samples. However, taking the average over all samples at a given temperature, yields a temperature-dependent trend, that is γ* is decreasing with increasing temperature as also shown in Figure S2 (b) exemplary for hFF03 + 1% hFF03-K17-Man + 5% hFF03-K17-RGD at 0.5 wt%.

Table S1. Critical deformations γ* determined from the amplitude sweeps at 25 °C (index 1) and 37 °C (index 2). The errors result from the fitting. The table also includes data, where it is not possible to determine a value for γ* (n.d. = not determined) and where data files were corrupted (f.c. = file corrupted).

name	*c* (wt%)	γ_1* (%)	γ_2* (%)
hFF03	0.15	7.1 ± 4.5	5.9 ± 2.1
	0.3	n.d.	12.1 ± 1.6
	0.5	12.4 ± 5.1	9.2 ± 1.2
hFF03-K17-Man	0.15	10.3 ± 5.1	8.1 ± 3.3
	0.3	13.3 ± 5.9	f.c.
	0.5	12.5 ± 2.3	12.3 ± 2.5
hFF03-K17-RGD	0.15	3.2 ± 1.7	3.0 ± 1.6
	0.3	9.3 ± 2.7	5.3 ± 3.3
	0.5	7.6 ± 1.9	7.2 ± 1.2
hFF03 + 1% hFF03-K17-Man	0.15	11.1 ± 4.8	f.c.
	0.3	11.6 ± 5.1	7.6 ± 1.8
	0.5	6.2 ± 2.3	6.8 ± 2.6
hFF03 + 5% hFF03-K17-RGD	0.15	7.7 ± 1.6	6.6 ± 1.4
	0.3	12.8 ± 3.6	2.2 ± 1.3
	0.5	f.c.	f.c.
hFF03 + 1% hFF03-K17-Man + 5% hFF03-K17-RGD	0.15	5.6 ± 1.9	2.0 ± 1.9
	0.3	4.9 ± 2.6	7.1 ± 3.7
	0.5	13.8 ± 2.9	10.3 ± 2.8

Comparing the phase angles δ(ω) at 25 °C and 37 °C no significant change is observed (see Figure S3), that is the gels have a unique elastic behaviour, which is not changed throughout changing the temperature.

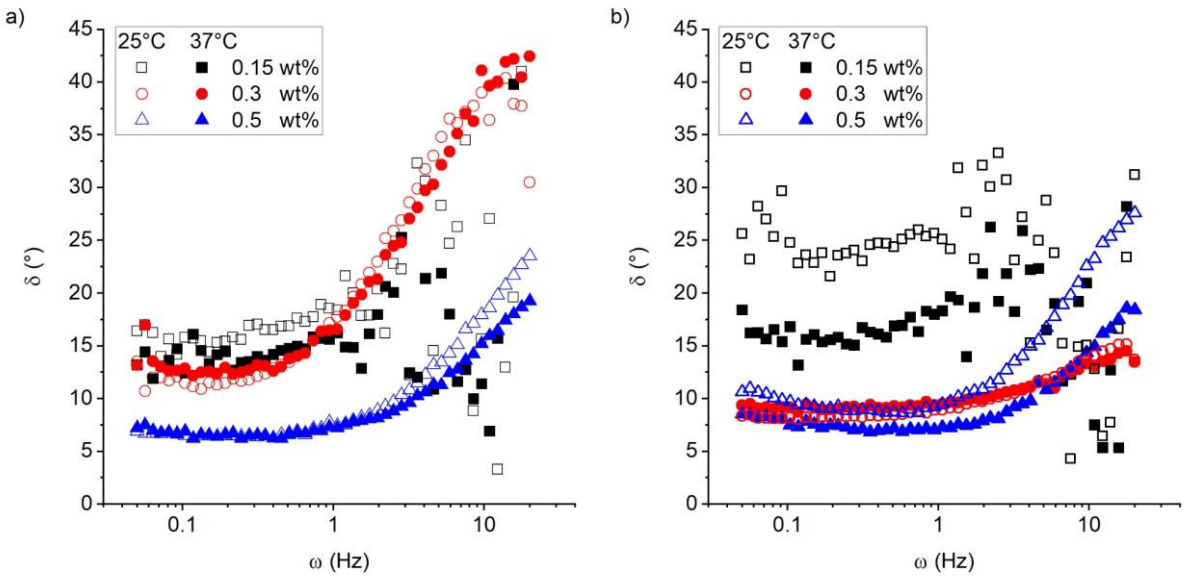

Figure S3. Phase angles of (a) hFF03 and (b) hFF03 + 1% hFF03-K17-Man + 5% hFF03-K17-RGD at different concentrations and temperatures.

For a detailed evaluation of the SANS data it is important to determine an approximate value for the length and the radius of one single peptide chain. It is assumed that the peptide units leucine, lysine, glutamate and alanine are of a spherical shape (see Figure S4).

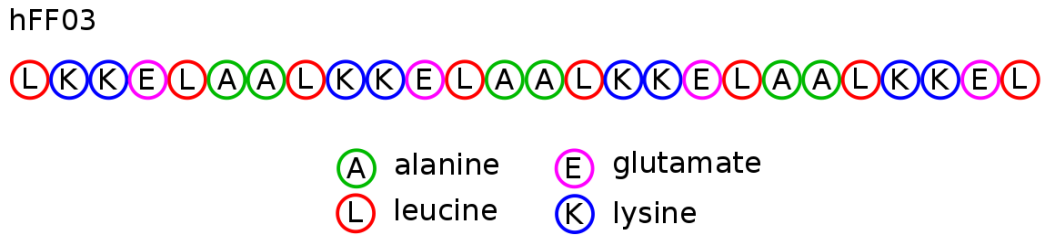

Figure S4. Schematic representation of a single peptide chain of hFF03 assuming the peptide units to be of spherical shape.

The molecular volumes V_{mol} are known from Y. Harpaz, M. Gerstein, C. Chothia, *Volume changes on protein folding*, Strucutre 2, 641 (1994), and can be converted to a radius R_u respectively diameter D_u. Further, the molecular weight M_w^u of each peptide unit is calculated from its chemical formula (see Table S2).

Table S2. Molecular volume V_{mol}, radius R_u and diameter D_u of a single peptide unit, number N_u of peptide units within one single chain and molecular weight of a peptide unit.

unit	abbr.	V_{mol} / Å³	R_u / Å	D_u / Å	N_u	M_w^u / g/mol
leucine	L	159	3.36	6.72	8	131
lysine	K	177	3.48	6.97	8	146
glutamate	E	178	3.49	6.98	4	147
alanine	A	108	2.95	5.91	6	89
arginine	R	211	3.69	7.39	1	174
glycine	G	91	2.79	5.58	1	75
aspartate	D	161	3.37	6.75	1	133
mannose	Man	270	4.01	8.02	1	180
glutar acid		200	3.63	7.26	1	132

The total theoretical length of a single peptide chain can be determined from summing over the corresponding products of D_u and N_u, yielding a value of L_{pep} = 172.87 Å or L_{pep} = 17.23 nm, respectively. Summing now over all products of V_{mol} and the corresponding N_u yields a value for the total volume of one single peptide chain, which is V_{pep} = 3498 Å³. Assuming a cylindrical shape of the peptide chain, it is possible to derive from V_{pep} and L_{pep} an effective radius of this chain, which is R_{pep} = 2.54 Å.

Besides the structural information, it is also necessary to determine the molecular weight of a single peptide chain. Hereby, the same procedure is used as described before, that is it is summed over the products of N_u and M_w^u, yielding for hFF03 a molecular weight M_w(hFF03) = 2891 g/mol. For the modified peptides molecular weights of M_w(hFF03-K17-Man) = 3203 g/mol and M_w(hFF03-K17-RGD) = 3237 g/mol are found.

The SANS data show a transition from a q^{-1} to a q^{-2} region at low q values indicating that rod-like structures are formed. The key information obtained from this transition region is the persistence length L_p. To extract this quantity the data are plotted in a Kratky-plot, that is $q^2 \cdot I(q)$ vs. q (see Figure S5). Within this plot, two regimes are to be distinguished, i.e. the q^{-2} slope reduces to a plateau value, while the q^{-1} reduces to a linear increase. From the cross-over q* of both regions the persistence length can be estimated as $L_p = 6/(\pi \cdot q^*)$. The corresponding values are listed in Table S3.

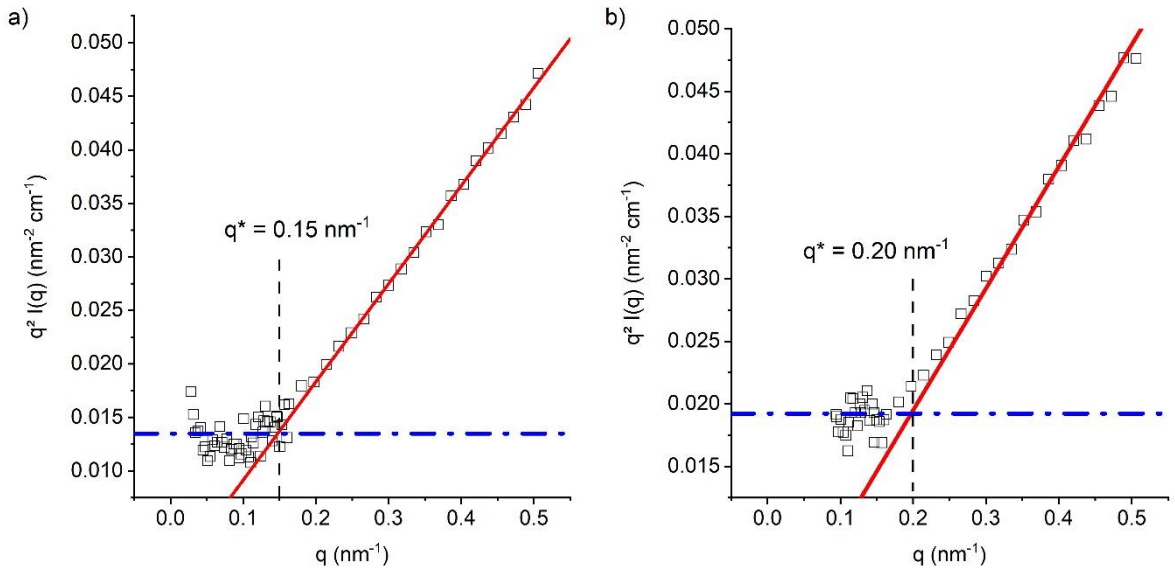

Figure S5. Kratky-plot of a) hFF03 and b) hFF03 + 1% hFF03-K17-Man + 5% hFF03-K17-RGD at 0.5 wt%. The straight lines indicate the different regimes of the q^{-2} and q^{-1} slope. The intersection point of both regimes is marked by q*.

Table S3. Persistence length L_p from the Kratky-plot and from fitting the scattering data with the Pedersen-Schurtenberger model (marked with (*)).

name	*c* (wt%)	L_p (nm)	L_p (nm) (*)
hFF03	0.5	13.0	9.8
	0.3	13.9	13.5
	0.15	15.1	9.2
hFF03-K17-Man	0.5	8.5	7.5
	0.3	15.4	8.9
	0.15	23.2	8.4
hFF03-K17-RGD	0.5	13.5	8.9
	0.3	13.7	10.0
	0.15	17.7	10.4
hFF03 + 1% hFF03-K17-Man	0.5	12.8	9.1
	0.3	14.7	12.7
	0.15	17.6	10.4
hFF03 + 5% hFF03-K17-RGD	0.5	10.3	7.0
	0.3	14.9	14.1
	0.15	16.6	9.8
hFF03 + 1% hFF03-K17-Man + 5% hFF03-K17-RGD	0.5	9.7	6.6
	0.3	21.6	12.3
	0.15	15.2	10.7

Further, it is possible to extract the molecular weight per unit length M_w^L from the SANS data. Therefore, a Guinier analysis is performed at the mid q-regime using Eq. (4) from which the pre-factor A corresponding to the forward scattering per unit length is extracted. The molecular weight per unit length is defined as

$$M_w^L / \text{ g/(mol Å)} = \frac{\rho^2 \cdot N_A \cdot A}{\pi \cdot (\Delta SLD)^2 \cdot c_g}. \quad \textbf{(S1)}$$

Hereby, ρ is the density, N_A the Avogadro constant, ΔSLD the difference of the scattering length densities of solvent (D_2O) and the peptide and c_g is the mass concentration of the peptide. Using the molecular weights calculated before for the different peptides as well as the length L_{pep}, it is possible to determine the molecular weight per unit length of one single peptide chain ($M_w^{L,chain}$). Dividing M_w^L by this determined value the number $N_{pep} = M_w^L/M_w^{L,chain}$ of peptide chains per cross-section can be estimated. The cross-sectional radius is determined through

$$R_{cs} \,/\, \text{nm} = \sqrt{\frac{M_w^L \cdot 10^{22}}{\pi \cdot \rho \cdot N_A}}. \quad \textbf{(S2)}$$

Hereby, M_w^L is taken in units of [g/(mol Å)] and ρ in units of [g/cm³]. The corresponding values are given in Table S4.

To supplement this assumption, the scattering data are also approximated using a model for a full and a hollow cylindrical form factor (see Figure S6 exemplary for hFF02 0.5 wt%). These approximations are compared to the Pedersen-Schurtenberger model as discussed in the main text. While the high and mid q regime are well reproduced by all three models, the cylindrical models fail a low q values, where the scattering data exhibit a q^{-2} to q^{-3} slope. Further, the model for the hollow cylinder reveals a core radius of 0.1 nm and a shell thickness of 1.0 nm, which seems unphysical assuming the core to be filled with water molecules having almost the same size as the channel formed.

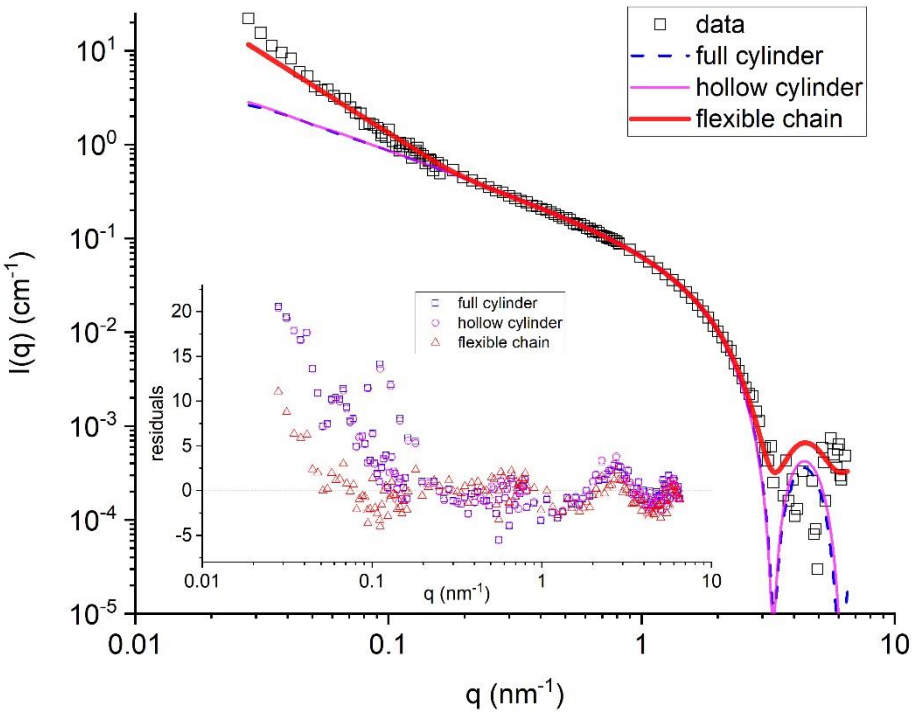

Figure S6. Scattering data of hFF03 0.5wt% fitted with the Pedersen-Schurtenberger model (red solid line) as well as with the model for a full cylinder form factor (dashed blue line) and a hollow cylinder (magenta solid line). The inset shows the error-weighted residuals of the fitting.

Table S4. Forward scattering intensity per unit length A as determined from a Guinier analysis of the scattering data, molecular weight M_w^L per unit length determined from Eq. (S1), number N_{pep} of peptide chains per cross-section, cross-sectional area A_{cs} and radius R_{cs} of the cross-section. The cross-sectional radius R_{cs} marked by (*) originates from fitting the SANS data with the Guinier model given in Eq. (4) and the values marked with (**) originate from fitting with the Pedersen-Schurtenberger model.

name	c (%wt)	c (g/cm³)	A (1/(cm Å))	M_w^L (g/(mol Å))	N_{pep}	A_{cs} (nm²)	R_{cs} (nm)	R_{cs} (*) (nm)	R_{cs} (**) (nm)
hFF03	0.5	0.005	0.009	311.9	19	5.18	1.28	1.30	1.14
	0.3	0.003	0.005	275.0	16	4.57	1.21	1.04	0.99
	0.15	0.0015	0.002	272.3	16	4.52	1.20	1.01	0.96
hFF03-K17-Man	0.5	0.005	0.016	553.0	30	9.19	1.71	1.24	1.18
	0.3	0.003	0.006	359.5	19	5.97	1.38	1.18	1.09
	0.15	0.0015	0.002	207.3	11	3.44	1.05	1.05	1.01
hFF03-K17-RGD	0.5	0.005	0.006	211.2	11	3.51	1.06	1.11	1.02
	0.3	0.003	0.003	147.3	8	2.45	0.88	1.30	1.09
	0.15	0.0015	0.002	194.7	10	3.23	1.01	0.74	1.01
hFF03 + 1% hFF03-K17-Man	0.5	0.005	0.010	362.3	22	6.02	1.38	1.16	1.14
	0.3	0.003	0.005	302.2	18	5.02	1.26	0.78	0.79

	0.15	0.0015	0.002	278.8	17	4.63	1.21	0.94	0.86
hFF03 + 5% hFF03-K17-RGD	0.5	0.005	0.011	368.4	22	6.12	1.40	1.16	1.14
	0.3	0.003	0.005	287.6	17	4.78	1.23	0.99	0.96
	0.15	0.0015	0.002	284.6	17	4.73	1.23	1.03	0.98
hFF03 + 5% hFF03-K17-RGD + 1% hFF03-K17-Man	0.5	0.005	0.010	352.8	21	5.86	1.37	1.16	1.14
	0.3	0.003	0.005	290.5	17	4.83	1.24	1.03	0.97
	0.15	0.0015	0.002	272.7	16	4.53	1.20	0.91	0.84

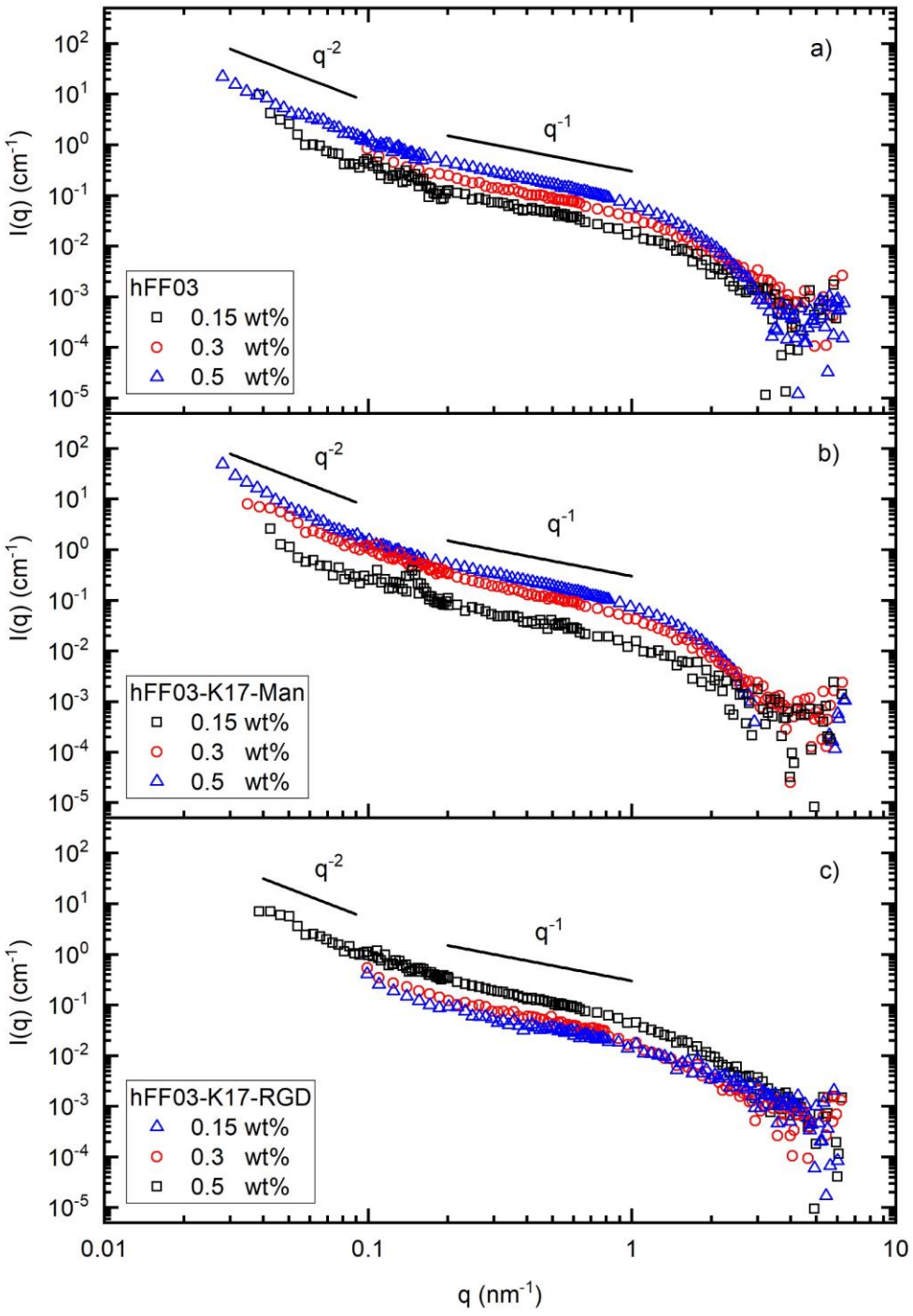

Figure S7. Scattering patterns of (a) hFF03, (b) hFF03-K17-Man and (c) hFF03-K17-RGD for different concentrations.

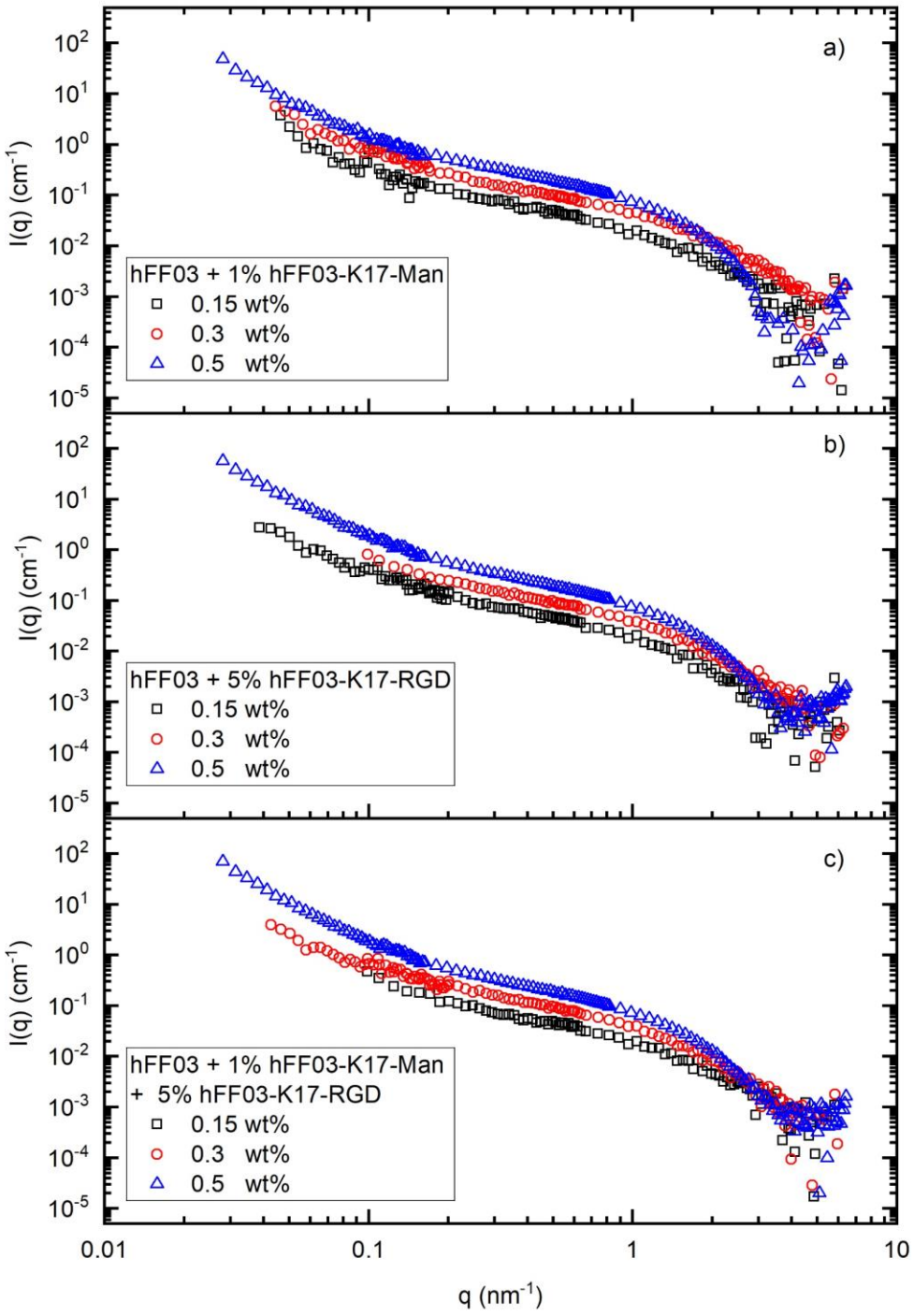

Figure S8. Scattering patterns (a) hFF03 + 1% hFF03-K17-Man, (b) hFF03 + 5% hFF03-K17-RGD and (c) hFF03 + 1% hFF03-K17-Man + 5% hFF03-K17-RGD at different concentrations.

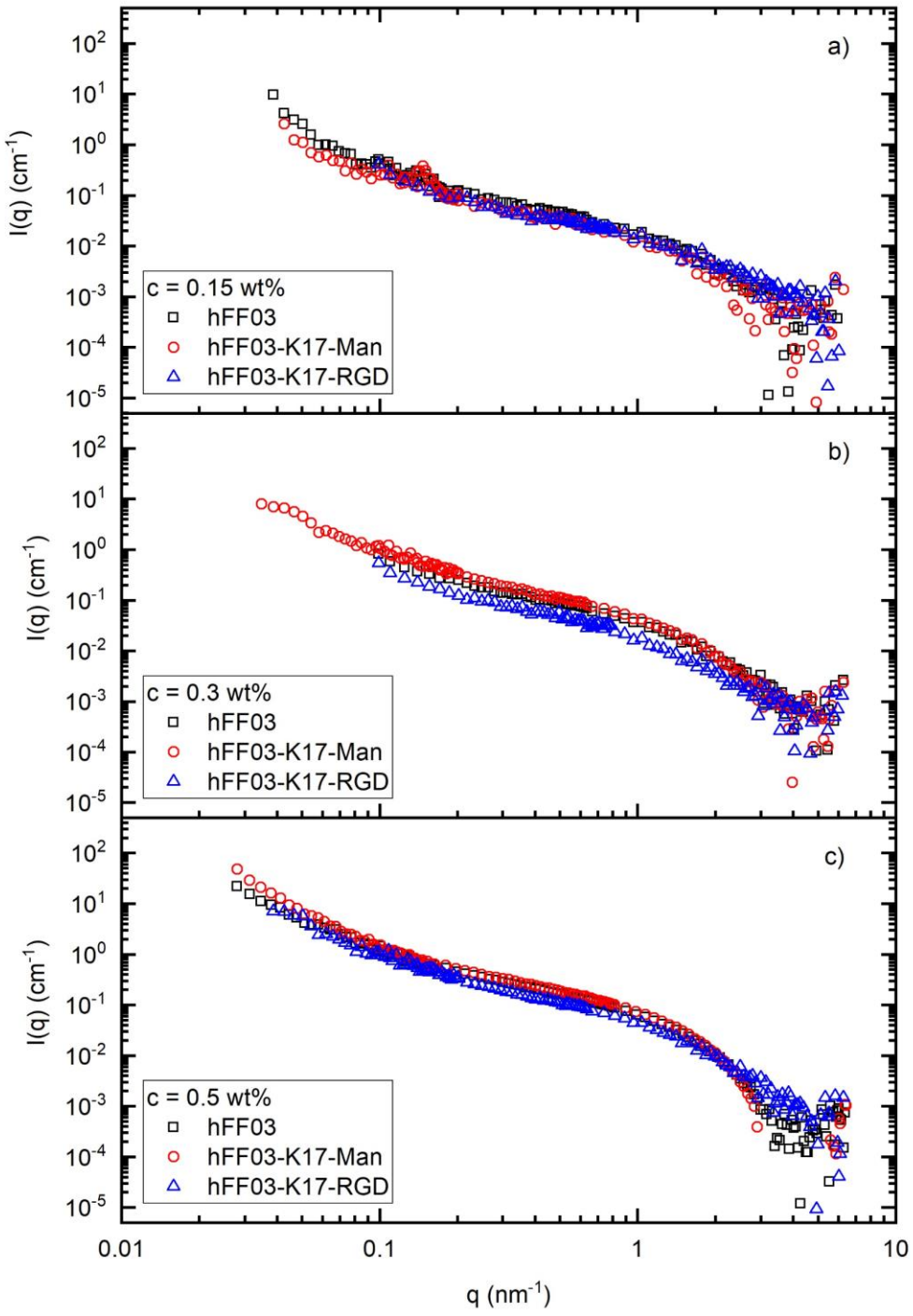

Figure S9. Scattering patterns of hFF03, hFF03-K17-Man and hFF03-K17-RGD group by concentrations (a) 0.15 wt%, (b) 0.3 wt% and (c) 0.5 wt%.

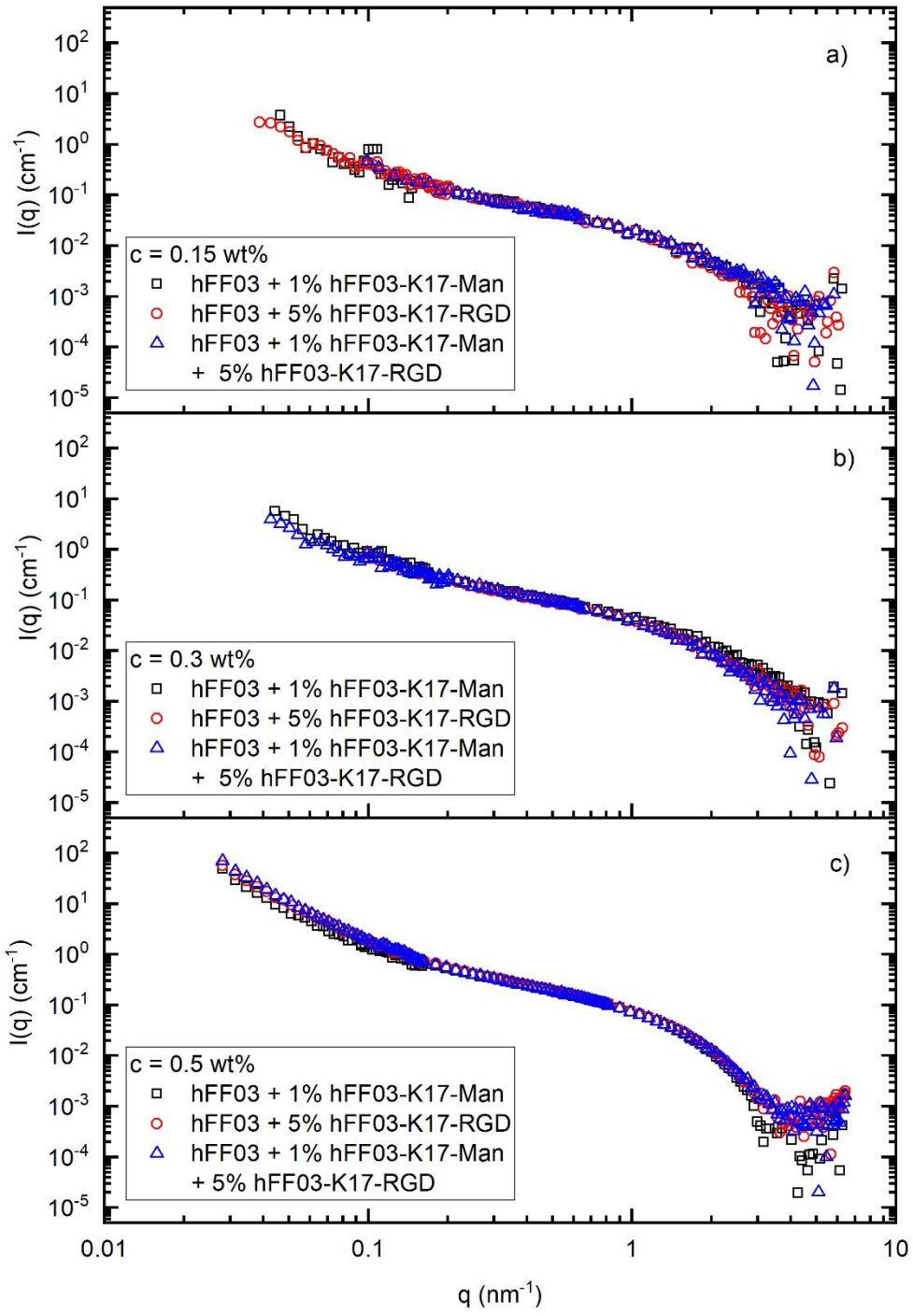

Figure S10. Scattering patterns of peptide mixtures hFF03 + 1% hFF03-K17-Man, hFF03 + 5% hFF03-K17-RGD and hFF03 + 1% hFF03-K17-Man + 5% hFF03-K17-RGD at (a) 0.15 wt%, (b) 0.3 wt% and (c) 0.5 wt%.

Table S5. Composition of tested pure peptide hydrogels and their mixtures. Addition of 1% and 5% ligand-presenting peptide refers to total concentration of hFF03 (WT).

Sample	wt%	hFF03 [μM]	hFF03-K17-Man [μM]	hFF03-K17-RGD [μM]
WT	0.15	498.37	-	-
	0.30	996.73	-	-
	0.50	1661.22	-	-
WT-CH	0.15	-	456.50	-
	0.30	-	913.00	-
	0.50	-	1522.00	-
WT-RS	0.15	-	-	449.41
	0.30	-	-	898.81
	0.50	-	-	1498.02
WT + 1% WT-CH	0.15	498.37	4.98	-
	0.30	996.73	9.96	-
	0.50	1661.22	16.61	-
WT + 5% WT-RS	0.15	498.37	-	24.92
	0.30	996.73	-	49.84
	0.50	1661.22	-	83.05
WT + 1% WT-CH + 5% WT-RS	0.15	498.37	4.98	24.92
	0.30	996.73	9.96	49.84
	0.50	1661.22	16.61	83.05